The Plant Cell, Vol. 18, 3617–3634, December 2006, www.plantcell.org © 2006 American Society of Plant Biologists

An Integrated View of Gene Expression and Solute Profiles of *Arabidopsis* Tumors: A Genome-Wide Approach [W]

Rosalia Deeken,[a] Julia C. Engelmann,[b] Marina Efetova,[a] Tina Czirjak,[a] Tobias Müller,[b] Werner M. Kaiser,[a] Olaf Tietz,[c] Markus Krischke,[d] Martin J. Mueller,[d] Klaus Palme,[c] Thomas Dandekar,[b] and Rainer Hedrich[a,1]

[a] Julius-von-Sachs-Institute, Department of Molecular Plant Physiology and Biophysics, University of Wuerzburg, D-97082 Wuerzburg, Germany

[b] Theodor-Boveri-Institute, Department of Bioinformatics, University of Wuerzburg, D-97074 Wuerzburg, Germany

[c] Institute of Biology II, Cell Biology, University of Freiburg, 79104 Freiburg, Germany

[d] Julius-von-Sachs-Institute, Department of Pharmaceutical Biology, University of Wuerzburg, D-97082 Wuerzburg, Germany

Transformation of plant cells with T-DNA of virulent agrobacteria is one of the most extreme triggers of developmental changes in higher plants. For rapid growth and development of resulting tumors, specific changes in the gene expression profile and metabolic adaptations are required. Increased transport and metabolic fluxes are critical preconditions for growth and tumor development. A functional genomics approach, using the Affymetrix whole genome microarray (~22,800 genes), was applied to measure changes in gene expression. The solute pattern of *Arabidopsis thaliana* tumors and uninfected plant tissues was compared with the respective gene expression profile. Increased levels of anions, sugars, and amino acids were correlated with changes in the gene expression of specific enzymes and solute transporters. The expression profile of genes pivotal for energy metabolism, such as those involved in photosynthesis, mitochondrial electron transport, and fermentation, suggested that tumors produce C and N compounds heterotrophically and gain energy mainly anaerobically. Thus, understanding of gene-to-metabolite networks in plant tumors promotes the identification of mechanisms that control tumor development.

INTRODUCTION

Integration and expression of oncogenes, encoded by the T-DNA of the *Agrobacterium tumefaciens* Ti plasmid, induce the development of plant tumors, also referred to as crown galls (Van Larebeke et al., 1974; Chilton et al., 1977). Rapid cell proliferation of tumors is promoted by high concentrations of cytokinin and auxin, which are synthesized by bacterial enzymes encoded by genes of the T-DNA (Kado, 1984). These plant growth factors not only control dedifferentiation of plant cells into primary tumor cells but also induce tumor cells to differentiate a vascular network of vessels and sieve elements. This network connects to vascular bundles of the host plant and thus sustains a rapid supply of nutrients and water (Malsy et al., 1992). Moreover, inevitable transpiration of noncutinized tumors with a disrupted epidermal layer drives nutrient flow into the tumor and mediates the accumulation of nutrients (Schurr et al., 1996; Wachter et al., 2003).

The growth of solid animal and human tumors also depends on neovascularization (Folkman, 1971; Gimbrone et al., 1974). Human tumors induce a dense network of blood vessels that supply the tumor with nutrients, water, and oxygen. Likewise, plant tumor cells proliferate only in vascularized regions, whereas in nonvascularized areas they necrotize (Ullrich and Aloni, 2000). Animal tumors overexpress angiogenic growth factors, such as tumor necrosis factor, fibroblast growth factor, and vascular endothelial growth factor, the latter of which is considered to be a major mediator in tumor angiogenesis (Risau, 1990; Carmeliet and Jain, 2000). In plants, gradients of growth factors such as cytokinins and auxin are established, inducing and controlling vascular differentiation (Aloni et al., 2003; Scarpella et al., 2006).

A common property of cancer cells is their capacity to metabolize glucose at high rates (Warburg, 1930; Aisenberg, 1961; Pedersen, 1978). Tumor mitochondria show impaired respiration, which is compensated for by an unusually high contribution of glycolysis to total ATP production. Some types of cancer have increased activity of the glucose transporter-1 (Chang et al., 2000), and its activity correlates inversely with survival (Wachsberger et al., 2002). The aberrant glucose metabolism provides a constant supply of energy even when oxygen levels decrease; as a result, the tumor has a metabolic growth advantage over normal tissues.

To attain a comprehensive picture of a T-DNA–induced plant tumor, we combine here bioinformatics and genome-wide expression analysis with direct analysis of metabolites, ions, oxygen consumption, and photosynthesis. The different data and approaches complement and strengthen each other and allow a detailed picture of the induced changes in the host cell from an

[1] To whom correspondence should be addressed. E-mail hedrich@botanik.uni-wuerzburg.de; fax 49-391-888-6157.
The author responsible for distribution of materials integral to the findings presented in this article in accordance with the policy described in the Instructions for Authors (www.plantcell.org) is: Rosalia Deeken (deeken@botanik.uni-wuerzburg.de).

[W] Online version contains Web-only data.

www.plantcell.org/cgi/doi/10.1105/tpc.106.044743

auxotrophic, aerobic metabolism to a heterotrophic, transport-dependent, sugar-degrading, and cell wall–synthesizing (gall formation) anaerobic metabolism.

RESULTS

In this work, we have studied alterations in the gene expression and solute content of *Arabidopsis thaliana* tumors and compared them with tumor-free inflorescence stalk tissue. When we analyzed the composition of metabolites of *Arabidopsis* tumors, we realized that their contents differed substantially from those of tumor-free tissue (see below). To understand the molecular mechanism causing these changes, we determined the gene expression profile of the transcriptome of *Arabidopsis* tumors. Because *Agrobacterium*-induced tumors might be composed of T-DNA–transformed and nontransformed cells responding to the altered milieu, the alterations in transcript levels and metabolite contents may reflect responses of both cell types. To interpret gene expression and metabolite data concerning tumor physiology correctly, we have used an in situ hybridization technique to calculate the percentage of transformed cells within *Arabidopsis* tumors. Using nopaline synthase (*NOS*) antisense RNA as a probe, >95% of tumor cells revealed a hybridization signal (reddish color in Figures 1A to 1D), indicating that they express *NOS* mRNA encoded by the T-DNA. However, this estimation differs from previous reports (see Discussion). Strong hybridization signals were observed in small and plasma-rich tumor cells (Figures 1A and 1C) but not in inflorescence stalk cells adjacent to the tumor (Figure 1B). In tumor cells with a large central vacuole, the hybridization signal was visible in the cytoplasmic border layers (Figure 1D, arrows). No signal was found in small or large tumor cells hybridized with the *NOS* sense RNA probe (Figures 1E and 1F, respectively). We cannot exclude the possibility that *Arabidopsis* tumors also contain a few nontransformed cells, but most cells appear transformed and express genes located on the T-DNA. Therefore, our studies of changes in gene expression and solute content reveal the results of the T-DNA integration event.

To analyze tumor gene expression data gained by microarrays (ATH1; Affymetrix), we checked the reliability of microarray data applying bioinformatics tools. After bioinformatic analysis (see below) of the transcriptome and biochemical analysis of the metabolome, we found concerted changes from autotrophic to heterotrophic metabolism in the tumor tissue. These involve the upregulation of genes involved in transport, glycolysis, sucrose degradation, and cell wall synthesis (for gall formation) as well as the downregulation of genes for photosynthesis, lipid metabolism, N metabolism, and amino acid synthesis. These results are described in detail below and are integrated into a comprehensive model (see Figure 9 below).

Bioinformatic Analysis of Affymetrix Microarrays

Data Acquisition

The Affymetrix microarray (ATH1 121501) was used to explore the differential expression profiles of genes in plant tumors induced by the nopaline-using *Agrobacterium* strain C58. Differentially expressed genes were identified from the expression data acquired from eight independent microarray hybridizations. Four replicates of tumor RNA and four of injured but not infected inflorescence stalks as reference RNA were used to calculate the expression value for each gene. Each replicate of four contained tissue fragments from at least 10 to 12 individual plants. For analysis of the expression profile, the fold change of normalized signals derived from tumor versus reference stalk tissue was calculated. Only fold changes of genes that met the significance criterion of $P < 0.01$ are presented here. Of 22,810 spotted genes on the *Arabidopsis* ATH1 microarray, 5054 (22%) met this criterion. Among them, 2340 genes (10%) were higher expressed in tumors (see Supplemental Table 1 online), and 2714 genes (12%) were higher expressed in reference inflorescence stalk tissue (see Supplemental Table 2 online). Of the 2340 genes with higher expression in tumors, 551 had a more than threefold difference, and of the 2714 with lower transcription, 608 were reduced at least threefold. The largest fold changes among all of the genes was a 56-fold ($P = 2.3E-04$) upregulation of an auxin-responsive GH3 family gene (At2g23170) and a 49-fold ($P = 1.2E-04$) downregulation in tumor tissues of the branched chain amino acid aminotransferase gene (At3g19710).

Clustering Microarray Data by Correspondence Analysis

Correspondence analysis revealed that the main difference between the eight microarray hybridization assays is attributable to differential expression between the two tissue types, tumor (T) and noninfected inflorescence stalk (N) tissue (Figure 2). This can be seen by the clear separation of the microarray assays from tumor and noninfected inflorescence stalk along the axis of the first component (*x* axis), confirming the high quality of the data. To examine whether the genes were also dispersed along the axis of the first component according to differential expression between tissue types, the locations of the 10 differentially expressed genes with lowest P values (Figure 2, circles) or highest fold changes (Figure 2, crosses) according to Linear Models for Microarray (LIMMA) analysis (Smyth, 2004) are highlighted in the correspondence analysis plot. Their positions at extreme values of the first component axis reflect differential expression of genes in different tissue types. Genes with the highest fold change are located at the outmost range of the first component, whereas genes with lowest P values have less extreme levels. The latter effect is attributable to the fact that genes with higher variance receive lower P values in the moderate *t* test analysis. This again indicates that genuine differential expression between tissue types is the strongest factor of variation in the data.

Functional Categorization

To structure the genes present on the *Arabidopsis* whole genome microarray, they were assigned to functional categories using the pathway analysis program MapMan (http://gabi.rzpd.de/projects/MapMan, version 1.8.0 [January 30, 2006]). MapMan is a user-driven tool that displays large data sets such as gene expression data from *Arabidopsis* Affymetrix microarrays onto diagrams of metabolic pathways or other processes (Usadel et al., 2005). Of 22,810 genes on the Affymetrix ATH1 chip,

13,642 (59.8%) could be assigned to categories with known biological functions (see Supplemental Figure 1 and Supplemental Table 3 online). The largest number of annotated genes of the ATH1 chip fall into the functional categories of protein and RNA.

To functionally categorize differentially expressed genes, we chose the 5046 genes with $P < 0.01$, which constituted ~22% of the 22,810 genes and gave a robust overview of differential gene regulation within functional categories. Among the 5046 genes selected, 3357 genes could be classified by MapMan into functional categories (see Supplemental Table 3 online). The distribution of these genes (total of 3357) within functional categories was compared with the distribution of all classified genes of the microarray (total of 13,642) and is presented as factorial changes in Figure 3. The factorial change describes the natural logarithm of the ratio of the percentage of differentially expressed genes in a functional category and the percentage of all annotated genes on the microarray in that category. For better comparison, the logarithmic factorial change of each category was plotted according to the following equation:

$$\text{factorial change} = \ln[(DE_{cat}/DE_{all})/(A_{cat}/A_{all})],$$

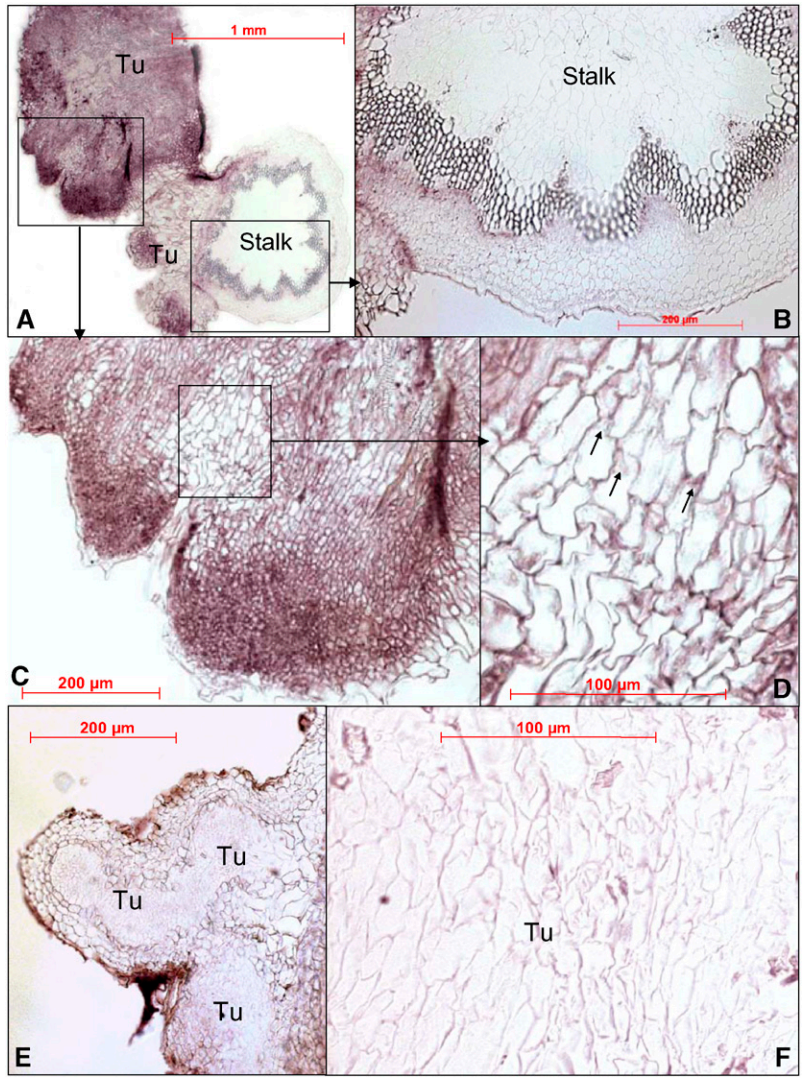

Figure 1. Detection of T-DNA–Transformed Cells in *Arabidopsis* Tumors.

(A) to **(D)** In situ hybridization using *NOS* antisense RNA as a probe.
(E) and **(F)** Hybridization with the sense RNA as a control. Positive hybridization signal appears as reddish color.
(A) Cross section through an inflorescence stalk (Stalk) and a tumor (Tu) attached to it.
(B) and **(C)** Enlargements of the marked areas in **(A)** of the inflorescence stalk and tumor.
(D) Enlargement of a tumor area with large cells marked in **(C)** showing hybridization signals close to the cell wall.
(E) Cross section of a tumor.
(F) Enlargement of a tumor area with large cells.

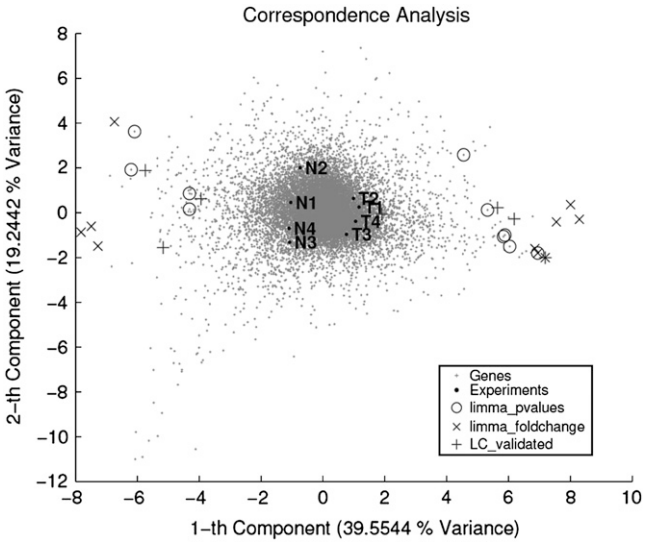

Figure 2. Correspondence Analysis of the Gene Expression Levels of the *Arabidopsis* Transcriptome.

Correspondence analysis shows that the main difference between the expression values of the different microarray hybridizations is attributable to differential gene expression between tumor and uninfected tissue. This can be seen from the separation of tumor and uninfected tissue microarray assays and differentially expressed genes along the horizontal axis. Genes are represented by tiny gray spots, and single microarray slides are indicated by black dots. N stands for reference slides, and T stands for tumor slides. Genes with lowest P values and highest fold change are marked with circles and crosses, respectively. Genes verified by RT-PCR are marked by plus signs.

where DE_{cat} represents differentially expressed genes in a functional category, DE_{all} represents all differentially expressed genes, A_{cat} represents all annotated genes in a functional category, and A_{all} represents all annotated genes on the array.

Thus, the factorial change represents a relative measure for overall gene regulation in a category. Functional categories with a positive factorial change have a higher fraction of differentially expressed genes than would be expected from the total number of genes assigned to that category. A negative value indicates a lower number of differentially regulated genes in the respective category than expected. Of the 17 functional categories shown in Figure 3, 11 contained a higher number of differentially expressed genes, whereas in six categories the number was lower. Categories 1 (photosynthesis [PS]), 36 (primary metabolism), and 34 (transport) were the three with a higher number of differentially expressed genes, in contrast with category 28 (DNA), in which a larger number of genes were not differently transcribed in the tumor and reference tissue (Figure 3; see Supplemental Table 4 online). The mean percentage of genes differentially expressed in a functional category was 28%, whereas in the DNA category, only 8% of the total gene number (882 genes) were significantly differentially expressed ($P < 0.01$; 71 genes). However, among the 71 significantly differentially expressed genes in the DNA category, 70% were activated in tumors. In the subcategory of DNA synthesis, even 73% of the genes involved in cell proliferation showed increased expression levels (cf. the subtables DNA_all and DNA_P < 0.0.1 in Supplemental Table 4 online).

Because the categories PS, primary metabolism, and transport were the three with the greatest number of differentially expressed genes, all annotated genes of the complete microarray belonging to these categories were assigned to subcategories (see Supplemental Figures 2A to 2C and Supplemental Tables 5 to 7 online). The greatest number of genes in the photosynthesis category was formed by the subcategory light reaction, and within the category of primary metabolism were major and minor CHO (carbohydrate metabolism) and mitochondrial e^- (electron) transport. In the category of transport, the subcategories ABC (for ATP binding cassette), metal, sugars, and metabolite contained the greatest number of differentially expressed genes.

The distribution of genes in these functional subcategories was again compared with the distribution of all differentially expressed genes of the microarray via factorial changes (Figure 4). Subcategories 14 (S assimilation), 12 (N metabolism), and 7 (oxidative pentose phosphate [OPP]) revealed the greatest number of differentially regulated genes, followed by subcategories 2 (major CHO), 5 (fermentation), and 4 (glycolysis) of the primary metabolism category (Figure 4A; see Supplemental Table 5 online). The greatest number of differentially expressed genes of the photosynthesis category belonged to subcategories 1.1 (light reaction) and 1.3 (Calvin cycle) (Figure 4B; see Supplemental Table 6 online). Among the 15 subcategories of the transport category, only two, 34.1 (P- and V-ATPases) and 34.8 (metabolite) contained a lower number of differentially regulated genes. It has to be mentioned that in the transporter subcategory metabolite, only mitochondrial membrane transporters are listed (see Supplemental Table 7 online). Because the four subcategories 9

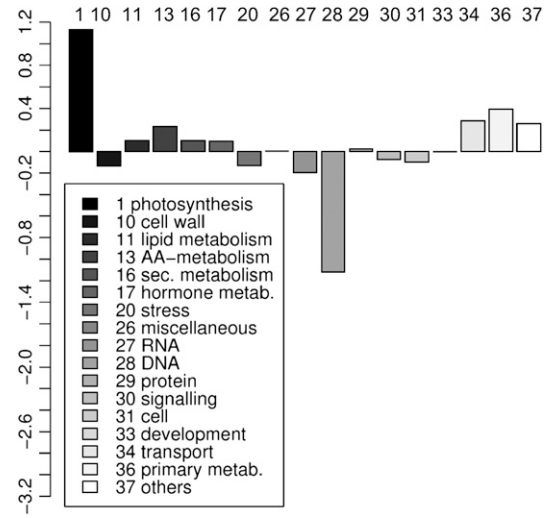

Figure 3. Factorial Changes within Functional Categories of All Differentially Expressed Genes.

The natural logarithm of factorial changes is plotted against each functional category. Positive factorial changes indicate a larger fraction of differentially expressed genes; negative factorial changes represent categories with a smaller fraction of regulated genes than expected from the total number of genes in the respective category. AA, amino acid.

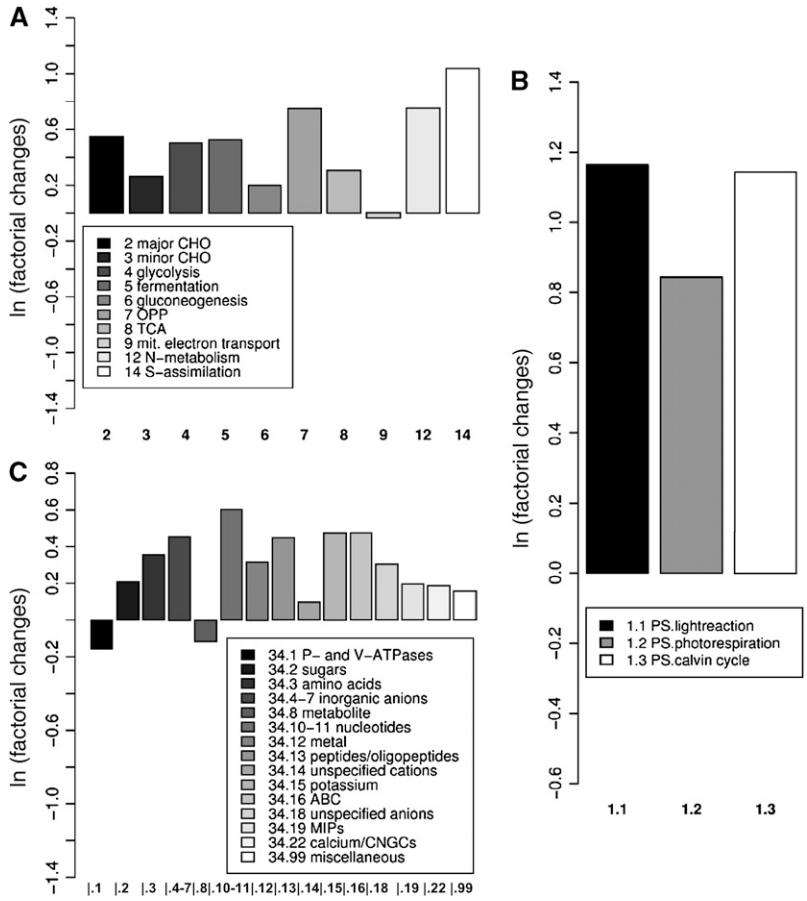

Figure 4. Factorial Changes of Functional Subcategories with the Highest Number of Differentially Expressed Genes.

The natural logarithm (ln) of factorial changes is plotted against the functional categories of photosynthesis **(A)**, primary metabolism **(B)**, and transport **(C)**. Positive factorial changes indicate more regulated genes; negative factorial changes indicate a smaller number of regulated genes in that category than expected from the size of the category. TCA, tricarboxylic acid; MIP, major intrinsic protein family; CNGC, cyclic nucleotide gated channel.

(mitochondrial e^- transport), 14 (S assimilation), 12 (N metabolism), and 7 (OPP) contain only a small numbers of genes, their factorial changes displayed in Figure 4A and in Supplemental Table 5 online are less reliable than those from the larger subcategories, such as 2 (major CHO) and 4 (glycolysis).

Members of the functional category transport are highlighted (black dots) in a MA plot (see Methods; Figure 5), because this category contained a large number of differentially expressed genes (Figure 3; see Supplemental Table 4 online). This plot shows that a considerable number of transporter genes with high mean intensities (high A values) are differentially expressed. These changes are referred to in more detail below.

Verification of Microarray Data by Quantitative RT-PCR

Numbers of transcripts of selected genes with either moderate or high differential expression values from microarray analysis were independently quantified by quantitative RT-PCR. They include a cytochrome oxidase (At5g56970), a wound-induced protein (At4g10270), a glycosyl hydrolase (At1g66280), a receptor protein kinase (At1g51805), a 2,4-D–inducible glutathione *S*-transferase (At1g78370), and a Ser carboxypeptidase I (At2g22990). The quantitative RT-PCR results of the latter six genes showed similar differential expression patterns as obtained by microarrays. Comparing the results of previous quantitative RT-PCR studies of *Arabidopsis* ion channel genes (Deeken et al., 2003) with those derived from the ATH1 microarray (KCO1, At5g55630; KCO2, At5g46370; KCO5, At4g01840; KCO6, At4g18160; KAT1, At5g46240; KAT2, At4g18290; AKT1, At2g26650; AKT2/3, At4g22200; At KC1, At4g32650; and GORK, At5g37500), a similar differential gene expression profile was obtained. Quantitative RT-PCR confirmed the microarray data. Of nine potassium channel genes of the *Arabidopsis* genome, two, AKT2/3 and GORK, were repressed in tumor tissues, whereas AKT1 and At KC1 were induced. Thus, both methods, microarray analysis and quantitative RT-PCR, revealed a high correlation between their identified fold changes of gene expression. The Pearson's correlation coefficient of microarray gene expression and quantitative RT-PCR data was 0.9453 ($P = 3.4E-8$) (see Supplemental Figure 3 online).

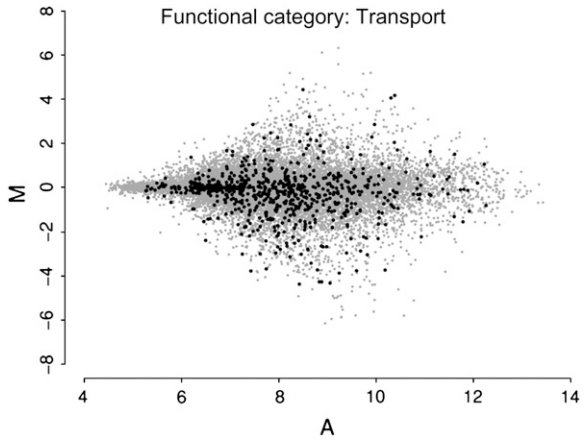

Figure 5. MA Plot of Genes of the Functional Category of Transport.

Many genes of the functional category transport are regulated between tumor and uninfected tissue. Regulated genes have large M values in the MA plot. The M values on the vertical axis represent differential expression between the two tissue types, and the A values on the horizontal axis represent average expression over all of the microarray assays. All genes are shown as gray dots, and genes of the functional category of transport are marked with black dots.

Solute Patterns and Gene Expression Profiles

Carbohydrate Metabolism and Photosynthetic Light Reactions

The carbohydrate pool (Figure 6) in tumor tissue was dominated by glucose (14.9 μmol/g fresh weight) compared with sucrose (2.8 μmol/g fresh weight) and fructose (1.7 μmol/g fresh weight) levels. Glucose concentration in tumors was 3.3 times higher than that in reference stalks (4.4 μmol/g fresh weight). Sucrose was found only in tumors and was undetectable in reference stalks.

Glucose accumulation in *Arabidopsis* tumors is most likely not derived from photosynthesis de novo, as transcript levels of the majority of differentially expressed genes ($P < 0.01$) related to photosynthesis were decreased (see Supplemental Table 4 online). This reflects the reduced number of chloroplasts in tumor cells that were smaller than those of mesophyll cells and the reduced expression of all genes encoded in the chloroplast genome (see Supplemental Table 6 online). A comparison of chlorophyll content revealed a three times reduced level in tumors compared with that in inflorescence stalk tissues (161 versus 499 μg chlorophyll *a/b* per gram fresh weight). This was paralleled by the downregulation of six genes out of seven involved in tetrapyrrole synthesis (see Supplemental Table 6 online). However, the relative quantum efficiency of chlorophyll fluorescence (Schreiber et al., 1986) was very similar in both tissues (0.67 ± 0.05 in tumors and 0.65 ± 0.04 in controls), which indicates that the still existing photosynthetic membranes were functional. Of 100 genes with differential expression ($P < 0.01$) involved in photosynthetic light reactions, all were significantly lower expressed in tumors. The same holds true for Calvin cycle genes (24 of 27; see Supplemental Table 6 online).

In tumor tissues, we found a strong activation of sucrose-degrading enzymes, accompanied by activation of *STP4* (At3g19930), a sink-specific monosaccharide transporter (see Supplemental Table 7 online), and increased glucose levels (Figure 6). The cluster of sucrose-degrading enzymes comprised 14 differentially regulated genes, of which 9 were activated. Most pronounced was the induction of two sucrose synthase genes (*SuSy3* [At3g43190] and *SuSy5.2* [At5g20830]), a fructokinase (At2g31390), and a cell wall invertase gene (At3g13790), whereas the genes of two vacuolar invertases were expressed to a much lower level in tumors (At1g12240 and At1g62660). Transcription of genes of the major CHO pathway coding for starch-synthesizing enzymes (7 of 10) and starch-degrading enzymes (13 of 14) was also reduced, again reflecting the reduced number of chloroplasts in tumor cells (see Supplemental Table 5 online).

Energy Production

Genes coding for proteins of mitochondrial electron transport were mainly unchanged in tumors, with the exception of an uncoupling protein, At PUMP1 (At3g54110), involved in the alternative respiratory chain, which was 2.6-fold ($P = 4.6E-04$) induced (see Supplemental Figure 5 and Supplemental Table 5 online). Genes required for fermentation were strongly upregulated: *Pyruvate Decarboxylase* (*PDC1* [At4g33070], $P = 1.2E-05$) and *Alcohol Dehydrogenase* (*ADH* [At1g77120], $P = 9.3E-05$). The increased transcript level of the latter two genes was paralleled by a threefold increase of ethanol concentrations in tumors (4.4 ± 1.5 μmol/g fresh weight) compared with reference stalk tissue (1.4 ± 0.4 μmol/g fresh weight), whereas lactate contents were not significantly different in both tissues. In addition, the oxygen uptake rate at air saturation of tumor tissue was 5.7 times higher per gram fresh weight (71 ± 31 versus 12 ± 3 $\mu mol \cdot g^{-1}$ fresh weight$\cdot h^{-1}$) and 3.8 times higher per gram of soluble protein (1622 ± 207 versus 427 ± 117 $\mu mol \cdot g^{-1} \cdot h^{-1}$).

Cell Wall Formation

The majority of genes (87 of 103) involved in cell wall synthesis, degradation, or modification showed increased expression in tumor tissue, of which 25 genes were more than threefold higher

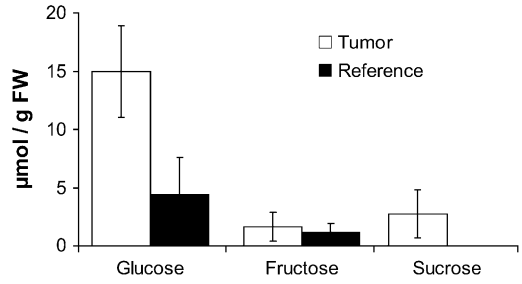

Figure 6. Sugar Content of *Arabidopsis* Tumors Induced by *Agrobacterium*.

Glucose, fructose, and sucrose were determined from tumors and tumor-free main inflorescence stalk segments (means ± SD; $n = 3$). FW, fresh weight.

expressed (see Supplemental Table 4 online). Among these were genes of the expansin family (At *EXP1* [At1g69530], P = 1.0E-04; At *EXP10* [At1g26770], P = 2.6E-03; At *EXP6* [At2g28950], P = 3.7E-03), the xyloglucosyl transferase family (At5g48070, P = 5.8E-04; At2g06850, P = 3.6E-04), the β-glucanase family (At1g70710, P = 4.6E-04; At4g02290, P = 3.4E-03), pectate lyases (At4g24780, P = 3.7E-03; At3g53190, P = 6.9E-04; At4g13210, P = 4.5E-05), cellulose synthase isoforms (At1g02730, P = 5.0E-04; At5g22740, P = 1.1E-03), members of the pectin esterases (At1g11580, P = 1.9E-04; At2g47550, P = 7.0E-04), polygalacturonase inhibitors (*PGIP1* [At5g06860], P = 3.1E-04; *PGIP2* [At5g06870], P = 2.9E-03), an α-xylosidase (At1g78060, P = 1.4E-03), a UDP-glucose-4-epimerase (At1g63180, P = 1.1E-03), and a polygalacturonase (At1g70500, P = 1.5E-04), indicating an increased reorganization and growth of cell walls.

Lipid Metabolism

Expression levels of the majority of genes involved in lipid metabolism were lower (68 of 101) in tumors than in inflorescence stalk tissue, except those belonging to the gene family of fatty acid desaturation. Genes of this family were higher transcribed in tumors, and three of five were induced even more than threefold (see Supplemental Table 4 online): a stearoyl acyl carrier protein desaturase (At1g43800, P = 7.5E-05), an ω-3 fatty acid desaturase (At2g29980, P = 4.2E-04), and a Δ-9 fatty acid desaturase (At2g31360, P = 4.4E-04). In addition, one gene of the lipid transfer protein family (LPT) showed 10-fold increased transcript levels (*LTP2* [At2g38530], P = 2.3E-04). The fact that tumors lack an intact epidermal cell layer covered by a cuticle is reflected by a 13-fold lower expression of *CUT1* (At1g68530, P = 1.5E-04) and a 4-fold lower expression of *WAX2* (At5g57800, P = 2.2E-04), two genes involved in cutin biosynthesis (see Supplemental Table 4 online).

N Metabolism

The total amino acid content in tumors was 8.4-fold higher than in inflorescence stalk tissue (Figure 7A). Among the proteinaceous amino acids, Gln was most prominently increased (14.7-fold). Furthermore, Ser, Asp, Glu, Thr, Pro, and Asn were increased severalfold in tumor tissues (6.4-, 6-, 3.1-, 6.5-, 11.7-, and 31-fold, respectively), and Ala, Val, Ile, Leu, His, and Arg were 25- to 7-fold higher in tumors than in controls.

Amino acids may accumulate in the tumor by import, de novo synthesis, and/or protein degradation. Uptake of amino acids into tumor cells might be mediated by two amino acid transporters (At1g47670, threefold, P = 8.9E-04; At1g25530, threefold, P = 5.0E-03) in addition to two H^+-dependent oligopeptide transporters (At4g21680, 17-fold, P = 1.6064E-05; At1g59740, 11-fold, P = 4.8E-04), the genes of which were strongly upregulated in tumor tissues (see Supplemental Table 7 online).

The first step in autotrophic N metabolism is the reduction of nitrate, which may be taken up by nitrate transporters into tumor cells. Transcription of two-high affinity nitrate transporter genes (At3g45060, 6-fold, P = 3.1E-04; At5g60780, 2-fold, P = 5.3E-03) was significantly induced in tumors, whereas that of low-affinity nitrate transporters, active in the millimolar range (*NTP2* [At2g26690], 0.13-fold, P = 9.5E-04; *NTP3* [At3g21670], 0.08-fold, P = 4.6E-05), was reduced severalfold (see Supplemental Table 7 online). The nitrate concentration (Figure 8A) was low in tumors (8 μmol/g fresh weight) and fivefold higher in reference tissues (41 μmol/g fresh weight). Expression of the two *Arabidopsis* nitrate reductase genes, *NR1* (At1g77760) and *NR2* (At1g37130), was 0.88 (P = 8.4E-02) and 1.45-fold (P = 6.0E-02), respectively, and thus not significantly different among both tissues. Corresponding to the nitrate content, the actual nitrate reductase enzyme activity was reduced fivefold in tumors. The maximal nitrate reductase activity was even 11-fold lower (Figure 8B). One gene encoding a mitochondrial Gly decarboxylase complex H (At2g35120), a source for photorespiratory ammonia, was 2-fold (P = 5.6E-03) higher in tumors, but two others (At2g35370, 0.13-fold, P = 9.9E-05; At1g32470, 0.53-fold, P = 7.9E-03) were strongly repressed (see Supplemental Table 6 online). Uptake of ammonium into tumor cells was most likely not facilitated by transporters, because the two differentially expressed ammonium transporter genes (*AMT2* [At4g13510], 0.54-fold, P = 2.5E-03; *AMT1.1* [At2g38290], 0.59-fold, P = 5.1E-03) and the only differentially expressed gene encoding a tonoplast-located aquaporin (*TIP2.2* [At4g17340], 0.13-fold, P = 2.8E-04) showed decreased expression levels in tumors (see Supplemental Table 7 online).

Among the 73 differentially expressed genes (P < 0.01) involved in amino acid metabolism (see Supplemental Table 4 online), only those coding for enzymes of Trp (*ASA1* [At5g05730], 3-fold, P = 5.2E-04; At5g38530, 3-fold, P = 3.2E-04) and Asp (At5g19550, 4.5-fold, P = 1.3E-04) biosynthesis were strongly induced in tumors, correlating with the increased level of Asp, but not that of Trp, which was below the detection level (Figure 7A). Although transcript levels do not necessarily correlate with enzyme activity, or with the accumulation of metabolites, this finding suggests an increased consumption of Trp in tumors, most likely as a precursor for auxin biosynthesis through enzymes expressed by the bacterial T-DNA. None of the membrane permease genes participating in auxin uptake (*AUX1* [At2g38120], *LAX1* [At5g01240], *LAX2* [At2g21050], *LAX3* [At1g77690]) or release (*PIN1* [At1g73590], *PIN2* [At5g57090], *PIN3* [At1g70940], *PIN4* [At2g01420], *PIN5* [At5g15100], *PIN6* [At1g77110], *PIN7* [At1g23080]) were significantly (P < 0.01) differentially expressed (see Supplemental Table 4 online). Genes of the ABC superfamily, coding for *p*-glycoproteins (PGPs), were recently shown to actively transport auxin (Geisler et al., 2005; Geisler and Murphy, 2006). Two genes of the PGP subfamily (At *PGP1* [At2g36910], 3-fold, P = 1.3E-03; At *PGP4* [At2g47000], 3-fold, P = 7.3E-04) were significantly expressed to a higher level in tumors (see Supplemental Table 2 online), indicating that auxin relocation in tumors might be controlled by this type of transporter.

The accumulation of Arg in tumors might be attributable in part to the differential expression (P < 0.01) of four genes involved in Arg metabolism. Three genes (At3g27740, P = 7.1E-03; At1g75330, P = 3.7E-03; At3g57560, P = 8.1E-03) coding for enzymes of Arg synthesis were upregulated (1.3- to 1.4-fold), but the only gene for Arg degradation, Arg decarboxylase 2 (At4g34710), was downregulated (0.72-fold; P = 4.4E-03) in

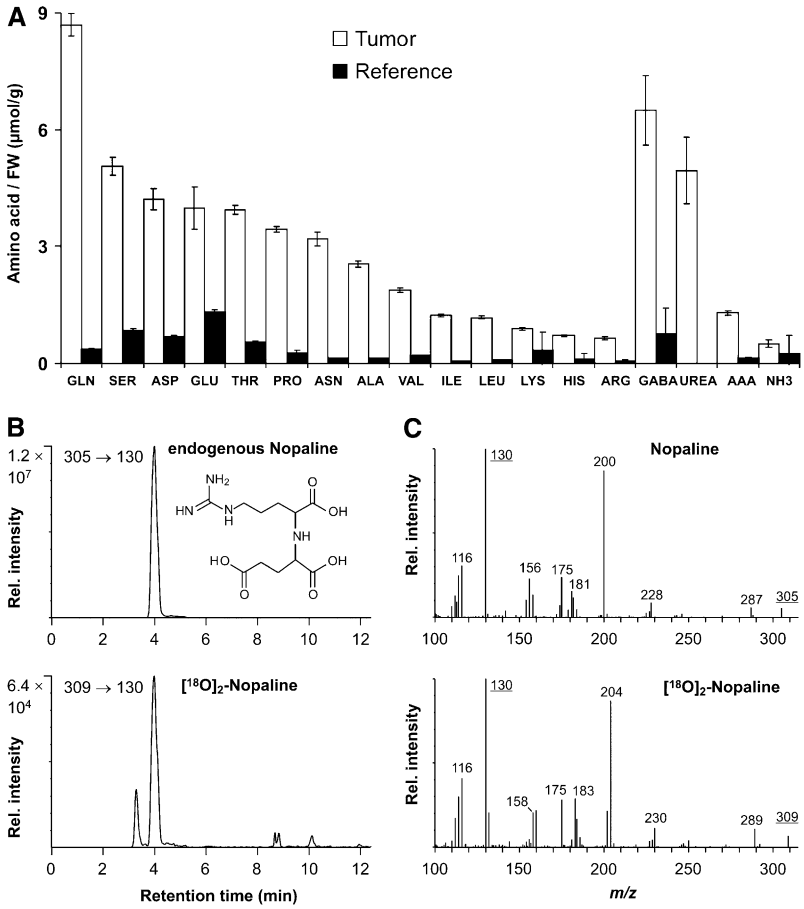

Figure 7. Content of N Components and Nopaline Determination of *Arabidopsis* Tumors Induced by *Agrobacterium*.

(A) Proteinaceous and nonproteinaceous amino acids were determined from tumors and tumor-free main inflorescence stalk segments (means ± SD; $n = 3$). FW, fresh weight.

(B) Multiple reaction monitoring ion chromatograms of an extracted *Arabidopsis* tumor sample. Mass chromatograms for the multiple reaction monitoring transitions at *m/z* 305 → 139 (endogenous nopaline) and *m/z* 309 → 139 ($[^{18}O]_2$-nopaline, internal standard) are shown. Endogenous nopaline levels were calculated from the ratio of the peak areas (nopaline:$[^{18}O]_2$-nopaline].

(C) Product ion spectra of $[M+H]^+$ of endogenous nopaline (*m/z* 305) and $[^{18}O]_2$-nopaline (internal standard, *m/z* 309). Retention times and spectra obtained from liquid chromatography–tandem mass spectrometry (LC-MS/MS) runs of nopaline extracted from tumor samples were identical to spectra of authentic reference compounds.

tumors (see Supplemental Table 4 online). Levels of nopaline, which is synthesized in transformed tumor cells from Arg, were determined in tumors by applying HPLC–electrospray ionization–mass spectrometry. Endogenous nopaline was unambiguously identified by its retention time and product ion spectrum of $[M+H]^+$ at *m/z* 305 (Figures 7B and 7C). Quantification in the multiple reaction monitoring mode was performed using $[^{18}O]_2$-nopaline as internal standard. Nopaline was found in *Arabidopsis* crown gall tumors in the millimolar concentration range (5.58 ± 1.89 μmol/g fresh weight; mean ± SD [$n = 4$]).

Most abundant among nonprotein N compounds were levels of γ-aminobutyric acid (GABA), α-aminoadipinic acid (AAA), and urea, which were either present in reference tissues in very low concentrations or not detectable (Figure 7). GABA accumulation might be explained by the strong induction of the Glu decarboxylase gene *GAD1* (At5g17330, sixfold, P = 3.3E-05). Urea is a product of nopaline degradation, catalyzed by arginase, an enzyme of *Agrobacterium*. Agrobacteria are present in the apoplast of growing tumors, and expression of the bacterial arginase gene within *Arabidopsis* tumors was confirmed by RT-PCR (data not shown). Uptake of urea into *Arabidopsis* tumor cells could be mediated by aquaporins, because it has been shown that at least the tobacco (*Nicotiana tabacum*) plasma membrane–located water channel, Nt AQ1, in addition to water, facilitated the transport of urea (Otto and Kaldenhoff, 2000). Two genes encoding plasma membrane–located aquaporins were severalfold higher expressed in tumors (*PIP2.5* [At3g54820], 12-fold, P = 3.3E-05; *PIP1.3* [At1g01620], 6-fold, P = 8.1E-05), whereas the urea transporter (At5g45380) was downregulated (see Supplemental Table 7 online).

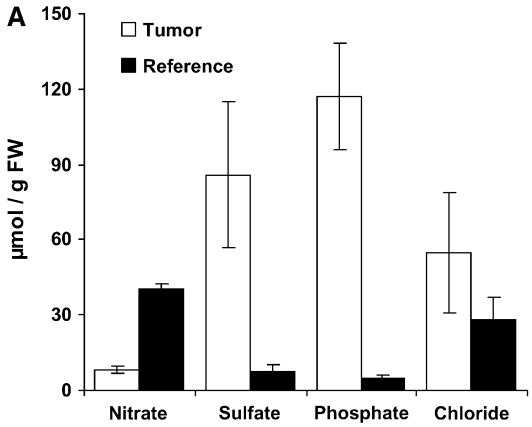

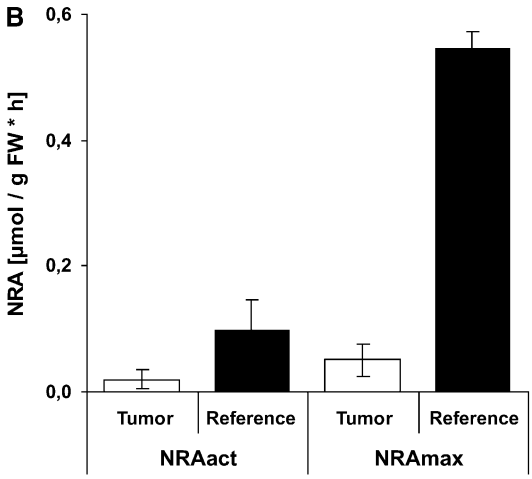

C

% Anions Located in the Apoplast		
Anion	**Tumor**	**Reference**
Sulfate	20.1 ±9.6	10.8 ±4.2
Nitrate	5.9 ±10,2	6.5 ±11.2
Phosphate	21.0 ±13.3	12.3 ±6.9
Chloride	25.8 ±18.3	9.7 ±3.6

Figure 8. Anion Content and Nitrate Reductase Activity of *Arabidopsis* Tumors Induced by *Agrobacterium*.

(A) Sulfate, nitrate, phosphate, and chloride were determined from tumors and tumor-free main inflorescence stalk segments (means ± SD; $n = 3$). FW, fresh weight.

(B) Comparison of the actual nitrate reductase activity (NRAact) and maximal nitrate reductase activity (NRAmax) of tumor and inflorescence stalk tissue (means ± SD; $n = 3$).

(C) Relative proportions of apoplastic anion to total anion contents of equally sized tumor and reference stalk tissue fragments.

Among the genes for amino acid degradation, only one, an osmotic stress–induced Pro dehydrogenase (At3g30775, four-fold, P = 1.0E-03) was prominently increased in tumors. In addition, more than half of the differentially expressed genes (65 of 126; $P < 0.01$), encoding enzymes of ubiquitin-dependent protein degradation, showed increased transcription in tumors (see Supplemental Table 4 online).

Inorganic Anions

Concentrations of sulfate and phosphate were increased in tumors (Figure 8A). The sulfate concentration was 12-fold higher in tumors than in reference stalk tissue. The phosphate content in tumor tissue reached 117 μmol/g fresh weight and was 23-fold enriched compared with that in the stalk. Chloride levels were increased in tumors (55 μmol/g fresh weight), but not significantly compared with the control stalks (28 μmol/g fresh weight). Because tumors show increased water loss and solute flow, certain anions might accumulate in the apoplast of tumors to a higher degree than in reference stalk tissue. As a crude approximation to apoplastic anion concentrations, we determined the relative anion content of the apoplast and found that the percentage of anions (except for nitrate) washed out of the apoplast within 10 min was approximately two times higher in tumors compared with inflorescence stalk segments of the same size (Figure 8C). All genes for sulfate transporters with $P < 0.01$ (At3g12520, At5g13550, At1g77990, At5g10180, At1g23090, At3g51895) were downregulated, whereas two of six coding for phosphate transporters (At1g26730, At1g14040) showed increased transcript levels (see Supplemental Table 7 online). This finding could indicate that tumor cells take up phosphate preferentially.

Finally, in a bioinformatic comparison, the tumor gene expression profile of the functional categories described above (photosynthesis, cell wall, lipid metabolism, amino acid metabolism, secondary metabolism, hormone metabolism, transport, primary metabolism, and tetrapyrrole synthesis from the category of others) was compared with the transcriptome of indole acetic acid– or zeatin-treated plant tissues (see Supplemental Table 8 online). These microarray data from the RIKEN Laboratory (Japan) are available at the AtGenExpress database (The Arabidopsis Information Resource [TAIR] accession: expression sets 100796604 and 1007965859) and revealed that a number of tumor genes (11 genes, P = 0.01; see Supplemental Table 8 online) were also differentially expressed after a 3-h treatment with indole acetic acid. The transcription of only two differentially expressed tumor genes (P = 0.01) was similarly regulated by zeatin, suggesting that auxin dominates the transcriptional regulation of tumor genes within the functional categories analyzed here.

DISCUSSION

This study shows that transformation of plant cells with T-DNA of the virulent *Agrobacterium* strain C58 results in genome-wide effects reflecting the adaptation of transport and metabolism. To our knowledge, a comprehensive transcriptome analysis of a crown gall tumor that integrates data of the tumor metabolome

had not been performed previously. A transcriptome study that focused on the timing of plant responses to short-term *Arabidopsis–Agrobacterium* interactions was performed recently. It shows that already at 48 h after inoculation of *Arabidopsis* cell suspensions with *Agrobacterium*, genes of the functional categories cell wall, primary metabolism, and protein/amino acid metabolism as well as transport were differentially expressed (Ditt et al., 2006). A comparison of the 303 regulated genes found by Ditt and coworkers with those of crown gall tumors revealed that 12% of the genes, irrespective of functional clusters, were regulated in both experiments. However, only 7% of these genes were similarly regulated, either activated or repressed ($P < 0.01$), in both data sets, when comparing only the genes belonging to the same functional clusters. This divergence in gene expression profile reflects the facts that (1) the study by Ditt et al. (2006) used a different plant system, (2) a different approach for the gene expression analysis was used, and (3) the gene set involved in the metabolism and transport of crown gall tumors differs even more from those of early signals of plant–pathogen interaction.

The question whether all tumor cells are transformed or most of them are only adapted to increased phytohormone levels produced by a few transformed cells has been addressed for almost 30 years. In earlier work, when no molecular markers were available, it was found that 1.2% of the cells were transformed (Sacristan and Melchers, 1977; Ooms et al., 1982). Later, Van Slogteren (1983) calculated by cloning of isolated axenic tumor tissues that 10 to 25% of the tumor cells were transformed. Recent studies, using β-glucuronidase (gus) gene–containing wild-type bacteria (A281p35S gus-int) and RT-PCR, provided strong evidence that in *Agrobacterium*-induced tumors, most cells, or even all cells (i.e., ~100%), were transformed (Rezmer et al., 1999). Here, using the *in situ* hybridization technique, a similar result was obtained. When several images, like those presented in Figure 1, were assessed visually by staining, >95% of the tumor cells were shown to express *NOS* mRNA. However, even if all cells are transformed, expression may be prevented by epigenetic phenomena as well. In fact, it has been shown that T-DNA–encoded genes can be inactivated through methylation (Gelvin et al., 1983; Amasino et al., 1984).

In the studies presented here, the metabolite and anion concentrations determined for whole tumors do not permit conclusions about their localization in bacteria, plant cell apoplast, or symplast, or about their subcellular distribution. However, gene expression analysis reflects exclusively the response of the plant cell. This study, using two different approaches, gene expression and solute analysis, indicates changes in the whole plant cell physiology. In a model of a plant tumor cell, we summarize the major changes in gene expression of transporters and metabolic pathways (Figure 9).

Nutrient Accumulation

Rapid growth of plant tumors creates strong metabolic sinks on host plants (Malsy et al., 1992; Pradel et al., 1996, 1999; Mistrik et al., 2000). In *Arabidopsis* tumors, almost all major nutrients were at higher concentrations than in the respective host tissues (Figures 6 to 8). However, some nutrients may appear specifically accumulated as a result of agrobacteria existing in developing crown gall tumors. Agrobacteria metabolize nopaline, synthesized by the transformed tumor cell, to Glu via Arg, Orn, and Pro (Dessaux et al., 1986). With the exception of Orn, the other three amino acids are markedly accumulated in tumors. However, in 1 mL of a suspension from the *Agrobacterium* strain C58 (OD = 0.873), a concentration that we have used for the induction of tumors, all amino acids were below the detection level. Even in 1 g of a bacterial pellet, the concentrations of the stress metabolites Pro, AAA, and GABA (see below), which accumulate in tumors, were not measurable (data not shown). Arg, the precursor of nopaline, was found in the bacterial pellet at a concentration of 0.44 μmol/g bacterial pellet, still slightly lower than in tumors (0.63 μmol/g fresh weight). Because the bacterial biomass in crown galls is much lower compared with that of plant cells, the contribution of bacterial Arg to the total content of Arg should be negligible in crown galls. Nopaline, which is synthesized by the T-DNA–encoded enzyme NOS, was found in tumors in the millimolar range. Because genes encoding enzymes of Arg synthesis were only slightly upregulated in *Arabidopsis* crown galls, their Arg content results most likely from translocation by the host plant via the transpiration stream. It has been shown that the content of several amino acids, including Arg, increases in the xylem sap of tumorized plants (Mistrik et al., 2000). Thus, amino acids do not reach the tumor only via the phloem but also via the transpiration stream. Moreover, Arg accumulation appears necessary, because the K_m of purified NOS for Arg is 0.74 mM (Kemp et al., 1979). This concentration is close to that measured in *Arabidopsis* tumors (0.63 mM).

Recently it was shown that the higher potassium concentration of *Arabidopsis* tumors was accompanied by the induction of root-specific K^+ channels in favor of shoot-specific channels (Deeken et al., 2003). A three times higher total anion concentration in tumors (266 versus 81 μmol/g fresh weight) might be the result of excessive transpiration and/or a lack of retranslocation from the tumor back to the plant. It has been shown that tumors are not covered by a cuticle and have a higher transpiration rate (Schurr et al., 1996), which might also cause the strong induction of the two water channel genes (Figure 9A). Thus, a high transpiration–driven solute movement may cause the accumulation of solutes in tumors (Wachter et al., 2003). Interestingly, most differentially expressed genes of anion transporters were downregulated in tumors (Figures 9B and 9C), indicating that part of the anions might actually be located within the apoplast. This hypothesis is supported by our observation that tumors lost a higher percentage of anions after 10 min of washing (Figure 8C). In addition, a higher protein content (55 ± 12 versus 33 ± 8 mg/g fresh weight) and neutral red staining (data not shown) indicated that tumors very likely possess more plasma-rich cells with smaller vacuoles. This suggests that anions most likely accumulate in the apoplast rather than in vacuoles of tumor cells. The uptake of nutrients into tumor cells is controlled by membrane transporters, of which a number of genes were differentially expressed between *Arabidopsis* tumors and tumor-free stalk tissues (Figures 3 and 4). Active transport is fueled by ATP hydrolysis, and in fact, two P-type H^+-ATPase genes (At4g30190, At1g80660) were upregulated, whereas all vacuolar ATPases were expressed at a lower level in tumors (see Supplemental Table 7 online). The latter might again support the

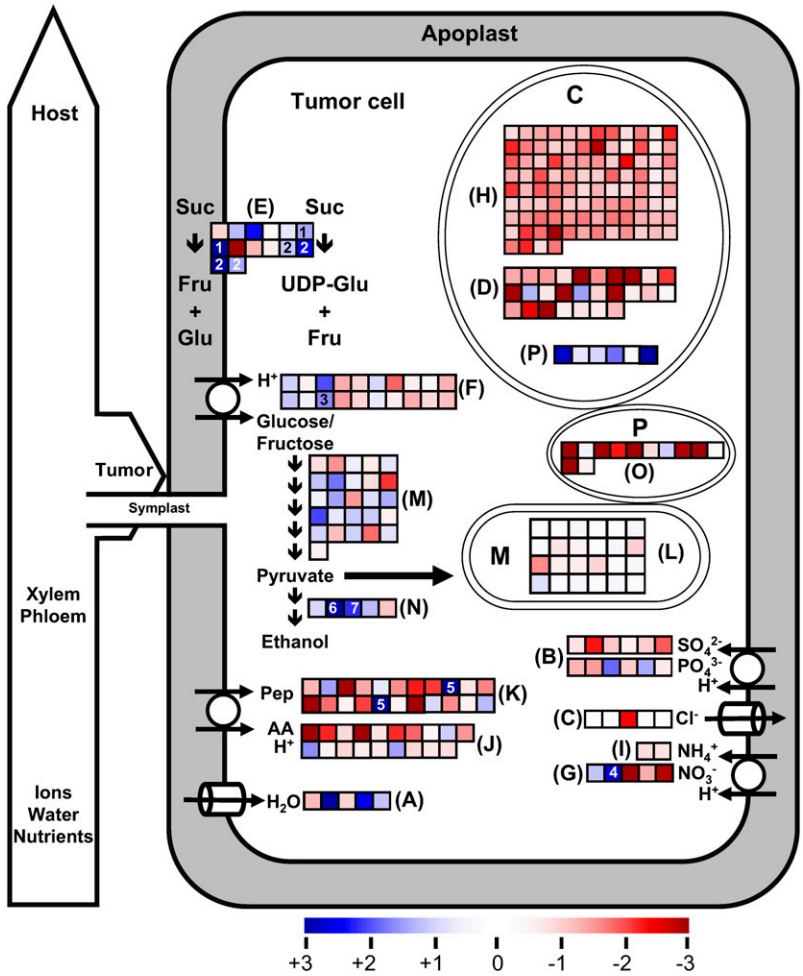

Figure 9. Scheme of Gene Expression Profiles of Transporters and Metabolic Pathways in *Agrobacterium*-Induced *Arabidopsis* Tumors.

Fold changes (log_2) of expression values of tumor versus inflorescence stalk tissues with $P < 0.01$ are presented as red (downregulated), blue (upregulated), and white (unchanged) squares for each gene, based on the pathway analysis program MapMan (https://gabi.rzpd.de/projects/MapMan/). Differential gene expression of water channels **(A)**, anion transporters **(B)**, chloride channels **(C)**, Calvin cycle enzymes **(D)**, sucrose degradation enzymes **(E)**, sugar transporters **(F)**, nitrate transporters **(G)**, light reaction enzymes **(H)**, ammonium transporters **(I)**, amino acid transporters **(J)**, peptide transporters **(K)**, electron transport enzymes **(L)**, glycolysis enzymes **(M)**, fermentation enzymes **(N)**, photorespiration enzymes **(O)**, and fatty acid desaturation enzymes **(P)** is shown. Numbers +3 to −3 on the color scale represent log_2 of the fold change. The flow of ions, water, and nutrients from xylem and phloem of the host plant into the tumor is indicated by the large open arrow. AA, amino acids; C, chloroplast; Fru, fructose; Glu, glucose; M, mitochondrion; P, peroxisome; Pep, peptide; Suc, sucrose; UDP-Glu, UDP-glucose.

notion that tumors possess a smaller vacuolar compartment. Another reason for metabolite accumulation might be that tumors are deprived of oxygen. It has been shown that roots that endure hypoxic stress accumulate sugars, amino acids, and GABA, as do the T-DNA–transformed tumor cells (Sousa et al., 2002).

Heterotrophic Metabolism

Glucose and amino acids appear to be the main carbon and nitrogen sources of the tumor. The C content calculated from sugars was 3.7 times higher in tumors than in tumor-free inflorescence stalks. De novo carbohydrate production should be low, as the transcription of the vast majority of the Calvin cycle genes was repressed (Figure 9D). Therefore, carbohydrates have to be supplied by the host plant, probably as sucrose via the phloem. The uptake of glucose into tumor cells is substantiated by an increased transcription of cell wall invertase and sucrose synthase (Figure 9E, 1 and 2) in addition to *STP4* (Figure 9F, 3), a sink- and pathogen-induced member of the monosaccharide transporter gene family (Truernit et al., 1996). An increased enzyme activity of acid cell wall invertase was described for tumors of *Kalanchoë*, tobacco, and *Ricinus* (Weil and Rausch, 1990; Pradel et al., 1999). It is a general phenomenon in the physiology of sink tissues to accumulate nutrients, although the expression of degrading enzymes is activated. This has been

reported by Wachter et al. (2003) for crown gall tumors of *Ricinus communis*, of which the high sucrose level in the periphery of the large tumor was accompanied by high cell wall invertase enzyme activity. These observations and our findings in *Arabidopsis* suggest that the influx of metabolites exceeds consumption in tumors.

Amino acid levels were eightfold higher in tumors compared with tumor-free tissue, whereas nitrate content was very low (8 ± 1 versus 41 ± 2 μmol/g fresh weight). Uptake of nitrate was not facilitated by anion transporters, because genes were downregulated except for two high-affinity-type transporters (Figure 9G, 4). The low nitrate content of tumors reflected the almost immeasurable nitrate reductase enzyme activity (Figure 8B). These findings confirm earlier data found by Mistrik et al. (2000), who have shown that tumors of *R. communis* have no detectable nitrate reductase activity, because of high levels of ethylene that inhibit nitrate reductase activity. In addition, abscisic acid, known to inhibit NO_3^- and PO_4^- uptake (Suleiman et al., 1990), was, as in *Ricinus* tumors (Mistrik et al., 2000), ~10 times higher in *Arabidopsis* tumors compared with uninfected inflorescence stalks (data not shown). Thus, a conclusion would be that increased amino acid levels probably are not attributable to higher nitrate assimilation. This is again substantiated by a reduced expression of genes involved in photosynthetic light reactions (Figure 9H) and by transporters for ammonium uptake (Figure 9I). The formation of ammonium from urea is most likely not favored in tumors, because transcripts of both urea-degrading enzymes appear not to be increased. Thus, nitrogen supply for amino acid and protein biosynthesis in tumors is most likely derived from Gln and Glu, which are translocated by the host plant through the vascular system and seem to be imported into tumor cells by amino acid transporters, of which three genes were induced in tumors (Figure 9J). In addition, peptide transport may provide another source of organic nitrogen. In tumors, two genes of oligopeptide transporters, one homologous with the *PTR1* gene from barley (*Hordeum vulgare*), were expressed (Figure 9K, 5). The PTR1 transporter was associated with peptide transport in germinating barley grains (West et al., 1998), which represent a sink tissue, like a tumor.

Anaerobic Energy Production in Tumors

Within the functional group photosynthesis, which includes photosynthetic light reactions, the majority of genes were strongly downregulated (Figure 9H). This implies less light-dependent oxygen production within the tumor, as confirmed by chlorophyll fluorescence. Expression of genes encoding the respiratory electron transport chain was mainly unchanged (Figure 9L) except for an uncoupling gene, At *PUMP1* (At3g54110). Suspensions of small tissue fragments from tumors gave a 5.7-fold higher oxygen uptake rate per gram fresh weight, or 3.8-fold higher on a protein basis, compared with stalk fragments. Because of their small size, these fragments in stirred solution probably were not limited by oxygen diffusion, and the higher oxygen uptake of tumor fragments over stalk fragments might reflect an uncoupling of respiratory electron transport. However, an intact tumor lacks intracellular air spaces. Thus, as a result of diffusional limitation together with an increased respiratory electron transport capacity, cells in the tumor core may easily become hypoxic. Under such conditions, plant cells switch to fermentative energy metabolism (Tadege et al., 1999). Genes coding for enzymes of the glycolytic pathway (Figure 9M) and ethanolic fermentation (Figure 9N) appear to prevail in tumors. Fructose seems to be the carbohydrate fed into the glycolytic pathway of tumors, because transcripts of two of three fructokinases (At2g31390, At4g10260) were 5.2-fold (P = 3.8E-04) and 2.4-fold (P = 1.3E-04) increased, whereas none of the genes that encode glucose-using enzymes was differentially expressed (see Supplemental Table 6 online). In addition, glucose was highly enriched in tumors, but fructose and sucrose contents were low (Figure 6). An increased ethanol level and the induction of *PDC1* transcripts (Figure 9N, 6) and *ADH* (Figure 9N, 7) confirm the switch to fermentation. The *PDC1* gene encodes the main regulatory enzyme of ethanolic fermentation and is also induced by abscisic acid (Kursteiner et al., 2003). In addition, it has been shown that genes involved in alcoholic fermentation, such as *ADH* (At1g77120), *PDC1* (At4g33070), and *PDC2* (At5g54960), showed a dramatic increase in expression under low-oxygen conditions in *Arabidopsis* roots (Klok et al., 2002). Both hypoxia and high abscisic acid levels might add to the induction of *PDC1* in tumors. ADH is also strongly induced by abscisic acid. These results imply that transformation of plant cells with T-DNA of the virulent *Agrobacterium* strain C58 is accompanied by a change from autotrophic to heterotrophic metabolism, in which ATP production is powered mainly by glycolysis and fermentation.

Stress Metabolites in Tumors

In addition to increased abscisic acid levels (see above), other stress metabolites, such as Pro, GABA, and AAA, were also strongly accumulated in *Arabidopsis* tumor cells (Figure 7) but were not measurable in pure agrobacteria. AAA might accumulate through the catabolism of Lys by the saccharopine pathway, which is important for the regulation of Lys homeostasis (Karchi et al., 1994). AAA is supposed to regulate growth, development, and responses to environmental changes by regulating the expression of genes involved in nitrogen metabolism (Arruda et al., 2000). In the case of osmotic stress responses, Glu, which is generated during Lys catabolism, might also act as a precursor of enhanced Pro biosynthesis. The increased Pro content (12-fold) was correlated with a strong repression of Pro oxidase (At5g38710). However, Pro dehydrogenase (At3g30775), another Pro-degrading enzyme, was induced, most likely as a result of increased Pro concentrations. Pro levels appear tightly controlled through feedback regulation (Kiyosue et al., 1996; Peng et al., 1996). GABA is probably increased as a consequence of anaerobic conditions within the tumor tissue, because oxygen deprivation and the resulting cellular acidosis strongly induce GABA accumulation (Kinnersley and Turano, 2000).

Signals derived from increased sugar levels lead to the inhibition of genes involved in photosynthesis, the Calvin cycle, and chlorophyll synthesis (Sheen et al., 1999; Pego et al., 2000; Smeekens, 2000). In *Arabidopsis* tumors, the vast majority of genes for light reactions (Figure 9H), the Calvin cycle (Figure 9D), and photorespiration (Figure 9O) show reduced transcription, in addition to genes encoded by the chloroplast genome (see

Supplemental Table 6 online). The latter reflects the reduced number of chloroplasts in tumor tissue. Whether that was attributable to the increased glucose remains unclear. The recent discovery of genes encoding enzymes of trehalose metabolism in higher plants has revealed trehalose-6-phosphate synthase and/or its product, trehalose-6-phosphate, as another potential player in sugar sensing (Rolland et al., 2001; Eastmond and Graham, 2003; Eastmond et al., 2003). Trehalose-6-phosphate synthase, of which the transcript levels of two members were strongly increased in *Arabidopsis* tumors (At1g23870, At2g18700), is required for embryo maturation and might also control developmental processes.

Expression of genes for the modification of fatty acids, such as desaturases (Figure 9P), and the transport of lipids, such as the lipid transfer protein LTP2 (At2g38530), was strongly increased in tumors. Within this group, some are involved in pathogen defense signaling. Stearoyl acyl-carrier protein desaturase (S-ACP-Des) catalyzes the initial step in fatty acid desaturation to form oleic acid. This monounsaturated fatty acid serves as a stimulator of phospholipase Dδ, which was shown to prevent cell death in parsley (*Petroselinum crispum*) suspension cells upon pathogen elicitation (Kirsch et al., 1997; Ryu, 2004; Wang, 2004) and modulates the activation of defense signaling pathways in plants (Kachroo et al., 2001, 2003, 2004). Activation of the S-ACP-Des gene in *Arabidopsis* tumors may help to prevent a hypersensitive response in defense against *Agrobacterium. Defective in Induced Resistance1* encodes a putative apoplastic LTP that is involved in systemic, but not local, resistance to pathogens (Maldonado et al., 2002). LTPs could also play a major role in cell wall modification. In tumors, they might shuttle lipids such as suberine monomers from their sites of biosynthesis through the plasma membrane into the cell wall, as suggested by Kunst and Samuels (2003), to minimize loss of water.

Auxin and Cytokinin May Control the Expression of Genes Involved in Tumor Metabolism

The differential expression of several of the genes discussed here may be regulated by auxin and cytokinin, two phytohormones that are known to be increased in crown gall tumors. Tumor cells are not only exposed to increased auxin and cytokinin levels for weeks but also to high levels of abscisic acid, ethylene, or jasmonic acid (Veselov et al., 2003). However, a comparison with the transcriptome of plant cells, treated with auxin and cytokinin for 3 h, indicated that the expression of at least 13 tumor genes (see Supplemental Table 8 online) might be regulated by auxin and cytokinin. The majority of these genes (10 of 13) are involved in phytohormone metabolism or signaling.

In conclusion, we have shown that plant tumors are characterized by anaerobic and heterotrophic metabolism and display an altered differentiation with modified, tissue type–specific gene expression patterns for photosynthesis, amino acid, cell wall, and lipid metabolism as well as for solute transporters. The transcription of several of these genes might be regulated by auxin and cytokinin. Metabolic changes and altered metabolite signaling seem to maintain vigorous growth of plant tumors after intrusion and successful transformation by agrobacteria.

METHODS

Plant Material and RNA Preparation

Arabidopsis thaliana plants (ecotype Ws-2) were cultivated in growth chambers under short-day conditions (8 h of light) at 22°C and 16°C during the dark period (16 h). Tumors were induced by applying the nopaline-using *Agrobacterium tumefaciens* strain C58 (noc^c) to the base of a wounded, very young inflorescence stalk (2 to 5 cm). At 35 d after infection, tumor tissue was separated from the host inflorescence stalk using a scalpel. Wounded but uninfected tumor-free inflorescence stalk segments of the same age served as reference tissues. To reduce data variation, total RNA was prepared from four independent biological replicates and used in four separate microarray hybridizations. Each replicate consisted of material from 10 to 12 individual plants. Total RNA was extracted from tumor and inflorescence stalk tissues and treated with DNase using the RNeasy plant mini kit (Qiagen) according to the manufacturer's protocol.

Probe Synthesis and in Situ Hybridization

Probes were generated by PCR using a 460-bp fragment of *NOS* cDNA and the following primers carrying a T7- or T3-RNA polymerase binding site at the 5′ end: NOSas-T7, 5′-CTTCTTTACCTATTTCCGCC-3′; NOSs-T3, 5′-TGATCCGATAGCTTAGACG-3′. Labeling with digoxygenin-11-dUTP of sense and antisense RNA strands was performed with the DIG-RNA labeling mix, applying either T7- or T3-RNA polymerase, respectively, according to the manufacturer's protocol (Roche Diagnostics). Labeled probes were dissolved in 100 μL of water. For hybridization, pieces of tumors with adjacent stalks were fixed in PBS + 4% paraformaldehyde at 4°C overnight, dehydrated in a series of increasing concentrations of ethanol and Histo-Clear (National Diagnostics), and finally embedded in paraffin at 60°C. Embedded material was cut with a microtome (Leica RM2245) in 9-μm sections and transferred to charged slides (Cnops et al., 2006). Samples were inspected with an inverted microscope (Axiovert 200M; Zeiss) and photographed with a digital camera (Axiocam MRC; Zeiss), applying the AxioVision LE software (Zeiss).

Microarrays and Data Preprocessing

A total of eight microarray slides (ATH1 121501; Affymetrix) containing the almost complete genome of *Arabidopsis* were used to monitor differentially expressed genes in tumor and inflorescence stalk tissue. Two different laboratories conducted two microarray hybridizations of each tissue type: (1) Nottingham Arabidopsis Stock Centre, Plant Science Division School of Biosciences, University of Nottingham, UK (http://www.york.ac.uk/res/garnet/providers); and (2) VBC-Genomics Bioscience Research, Vienna, Austria (www.vbc-genomics.com). Altogether, four arrays were hybridized with four different samples of tumor RNA and four with four different samples of inflorescence stalk RNA.

Data preprocessing was performed using Bioconductor software (Huber et al., 2002; Gentleman et al., 2004) running under the statistical programming environment R (Ihaka and Gentleman 1996). To obtain a normalized gene expression value from oligomer intensities for each gene of each microarray slide, variance stabilization (Huber et al., 2002) was applied. Variance stabilization calibrates for variations between the arrays through shifting and scaling and transforms the intensities to a scale on which the variance is approximately independent of the mean intensity. Before applying variance stabilization, no background correction was performed to the Affymetrix probe intensities, according to recommendations in the variance stabilization manual, and only the perfect match probes were used to compute the expression values for individual genes.

For summarization of probe intensities into gene expression values, we applied the median polish algorithm (D. Holder, R.F. Raubertas, V.B. Pikounis, V. Svetnik, and K. Soper, unpublished data), which is also incorporated into the commonly used robust multiarray analysis by Irizarry et al. (2003).

Assessing the Quality of the Data

To examine the quality of the microarray data, we applied three independent methods: two statistical methods (scatterplot and correspondence analysis) and one biological method (quantitative RT-PCR). First, the reproducibility of the individual Affymetrix microarray hybridizations was checked by scatterplot analyses. Normalized expression values of all genes of one microarray were plotted versus the expression values of another microarray. The scatterplots comparing two uninfected inflorescence stalk or tumor tissues with each other (see Supplemental Figure 4 online) displayed the variability of repeated measurements. The average correlation coefficients for the six scatterplots each of tumor and reference stalk arrays were 0.9725238 and 0.9623506, respectively. Thus, expression signals of genes from the same tissue type showed high consistency. The 12 scatterplots resulting from a comparison of tumor versus reference arrays indicated differentially expressed genes (see Supplemental Figure 5 online, red dots). Here, the average correlation coefficient was 0.86326 and indicated that many more genes differ between two microarray hybridizations of different tissue types.

In the next step, the reproducibility of chip hybridizations was confirmed by applying correspondence analysis. Correspondence analysis was conducted using a self-made script within MATLAB (MathWorks). Correspondence analysis represents genes as numerical vectors, with the number of elements of a vector being the number of microarray assays considered. Those vectors are projected into a lower dimensional subspace (typically, two dimensions) that accounts for the main variance in the data such that distances among points reflect their original distances in the high-dimensional space as closely as possible (Fellenberg et al., 2001). The same reduction of dimensions is done for the microarray assays; here, a 22,810-dimensional vector (of genes) is reduced to lower dimensions. By embedding both genes and assays in the same graph, correspondence analysis finds the most pronounced factor of differences between genes and microarray hybridizations.

Differential Gene Expression Analysis

To give a first graphic overview of differential gene expression between tumor and inflorescence stalk tissue, we performed an MA plot on gene expression data (Figure 5). In such an MA plot, the difference of log expression values (Minus) of the two tissue types [$M = \log(\text{tumor}) - \log(\text{reference})$] is plotted against the sum (Add) of the log expression values divided by 2 [$A = \{\log(\text{tumor}) + \log(\text{reference})\}/2$]. Thus, the *x* axis represents the extent of expression levels and the *y* axis represents differential gene expression.

For the statistical evaluation of differential expression between the two tissue types, we used a moderate *t* statistic implemented in the LIMMA package, which is part of the Bioconductor software project (Gentleman et al., 2004; Smyth, 2004). We applied the function lmFit() in the LIMMA software package to fit linear models on the expression values of each gene with the factors tissue type and laboratory. The function eBayes() was used to compute moderated *t* statistics by empirical Bayes shrinkage of the standard errors toward a common value. The advantage of the LIMMA package is its robustness and suitability for experiments with small sample numbers. Four repeated microarray hybridizations of each tissue type are not enough repeats for stable predictions using standard statistical *t* test analyses. To circumvent this limitation, the Bayesian functions were applied, exploiting information across genes and balancing the lack of more repeats needed for a classical *t* test. Thus, analyses with the LIMMA package are still stable with a small number of arrays (Smyth, 2004). The null hypothesis of differences between tissues being equal to zero was tested under the assumption of independent errors following a normal distribution. For each gene, we calculated a fold change and a P value measuring the statistical significance of differential expression. The significance level was corrected for multiple testing by applying the false discovery rate from Benjamini and Hochberg (2000). All of the P values given are corrected for multiple testing.

Fold changes of significantly differentially expressed genes ($P < 0.01$) were analyzed with the pathway analysis program MapMan. MapMan is a user-driven tool that displays large data sets (e.g., gene expression data from Affymetrix microarrays) onto diagrams of metabolic pathways or other processes (Thimm et al., 2004; https://gabi.rzpd.de/projects/MapMan/). A color code symbolizes the fold change of differential gene expression, where blue indicates higher expression in tumors and red indicates higher expression in inflorescence stalk tissue (Figure 9).

Comparison of Tumor- and Phytohormone-Dependent Gene Expression

Differential gene expression discussed for crown gall tumors was compared with two Affymetrix microarray data sets addressing differential expression arising from phytohormone treatments. Both data sets were produced by the RIKEN Laboratory (Japan) and are available at the AtGenExpress database. One data set includes the comparison of seedlings treated with indole acetic acid for 3 h with untreated seedlings (TAIR accession: expression set 100796604), the other set compares gene expression of seedlings treated with zeatin for 3 h with untreated seedlings (TAIR accession: expression set 1007965859). In both microarray data sets, there are two biological replicates of each treatment group, leading to a total of four microarray assays per data set. We analyzed the raw data (Affymetrix CEL files) in the same way as the tumor data, using variance stabilization normalization and LIMMA for differential gene expression analysis. Consistent with the P criterion for the crown gall tumor gene expression data set, genes with a multiple testing corrected $P < 0.01$ were considered differentially expressed. Although the lower number of replicates in the phytohormone data sets results in higher P values in the differential gene expression analysis, the P criterion was kept constant for consistency.

Quantitative Real-Time RT-PCR

Total RNA was extracted from tumor and stalk tissue with the plant RNeasy extraction kit (Qiagen). Poly(A)$^+$ RNA was isolated from total RNA with Dynabeads according to the protocol of the Dynabeads mRNA Direct kit (Dynal). To eliminate contamination with genomic DNA, poly(A)$^+$ RNA samples were treated twice with Dynabeads. First-strand cDNA synthesis and quantitative real-time RT-PCR experiments were performed as described previously (Szyroki et al., 2001) using LIGHTCYCLER 3.1 (Roche). Primers used were as follows: cytokinin oxidase (At5g56970), 5′-GATAGTTTAAACCATGT-3′ (forward), 5′-CAAAACTTCAGTATTTCC-3′ (reverse), 390 bp; wound-induced protein (At4g10270), 5′-TGGAACTACATACTCCG-3′ (forward), 5′-AATTTGAGTCACATTGAT-3′ (reverse), 316 bp; glycosyl hydrolase (At1g66280), 5′-GACACAACTACATTTGGA-3′ (forward), 5′-AACAGCAACAGAATCT-3′ (reverse), 390 bp; receptor protein kinase (At1g51805), 5′-TGGTTCTGTGTGGAAA-3′ (forward), 5′-AATCTACCTAGCCATTG-3′ (reverse), 214 bp; 2,4-D–inducible glutathione *S*-transferase (At1g78370), 5′-TTATTGAGGCAGTGAAG-3′ (forward), 5′-CGCATTATTAGGGGAA-3′ (reverse), 352 bp; Ser carboxypeptidase I (At2g22990), 5′-GGATCCATCTAACACAC-3′ (forward), 5′-AAGCTCTCGTGTATCCA-3′ (reverse), 446 bp. The number of transcripts was normalized to the constitutively expressed Actin2/8 mRNA (An et al., 1996).

Measurements of Solutes

Contents of amino acids, sugars, and anions were determined from aqueous extracts of 20 mg of fresh tumor or inflorescence stalk tissue. Amino acids were quantified with an amino acid analyzer (LC5001, Biotronic; Eppendorf-Nethler-Hinz), sugars by HPLC (Dionex series 4500i chromatography system), and anions by ion chromatography (IC 1000; Biotronic). For extraction of apoplastic anions, fresh tumor or inflorescence stalk tissues were cut into small pieces (2 to 3 mm) with a razor blade and briefly incubated in a large volume of water for 10 to 15 s to remove contamination of destroyed cells on the surface of the tissue. After incubation for 10 min in 1 mL of deionized water, the anion content of the washing solution was measured. Ethanol and lactate were determined enzymatically from 70 to 100 mg of fresh plant tissue (Roche Diagnostics).

Quantification of Nopaline

Synthesis of $[^{18}O]_2$-Nopaline Standard

Labeled nopaline was synthesized through an acid-catalyzed oxygen-exchange reaction according to a previously described procedure (Mueller et al., 2006). Briefly, unlabeled nopaline (25 μg) was dissolved in 50 μL of $H_2^{18}O$ (99 atom % ^{18}O; Isotec). After addition of 50 μL of a 4 M HCl solution in 1,4-dioxane (premade solution; Aldrich Chemicals), the sample was incubated in a tightly closed screw-cap vial for 1 h at 60°C. Thereafter, the sample was dried in vacuum, dissolved in methanol, and stored at −20°C. Theoretically, all six oxygens of the three carboxyl groups of nopaline can be exchanged by ^{18}O through this procedure. Because of the instability of nopaline in the acid-exchange medium, incubation was terminated after 1 h when the majority of the recovered nopaline was labeled with two ^{18}O atoms and unlabeled nopaline became undetectable. In addition to $[^{18}O]_2$-nopaline, the mixture also contained labeled nopaline molecules with one to four ^{18}O atoms; these, however, did not interfere with the analysis. $[^{18}O]_2$-Nopaline was quantified against unlabeled nopaline and used as an internal standard.

Plant Extraction and LC-MS/MS Quantitation of Nopaline

For nopaline analysis, frozen plant material (50 mg) was mixed with 750 μL of a pre-warmed mixture (75°C) of methanol:water (75:25, v/v). After addition of a ceramic bead (6 mm in diameter), the tissue was homogenized and extracted using a vibrating ball mill for 1 min. After an incubation period of 1 min at 75°C, 250 ng of the internal standard, $[^{18}O]_2$-nopaline, was added and homogenization was repeated. Thereafter, the sample was centrifuged (1000*g* for 10 min), and the supernatant was dried in a vacuum centrifuge at 50°C. The residue was suspended in acetonitrile:water (20:80, v/v). After centrifugation (1000*g* for 2 min), the supernatant was transferred into an HPLC vial, and 10 μL was injected into the LC-MS/MS system. LC-MS/MS analyses were performed using a 1200 Agilent HPLC system coupled to a Micromass Quattro Premier triple-quadrupole mass spectrometer (Waters). The column (Phenomenex Synergi Hydro-RP, 150 × 4.6 mm, particle size, 4 μm) was eluted with a linear mobile phase gradient (0.5 mL/min flow rate) starting from water containing 0.1% formic acid at 0 min to acetonitrile:water:formic acid (20:80:0.1, v/v) at 10 min. The mass spectrometer was operated in the ESI+ mode using multiple reaction monitoring. Argon was used as collision gas (22 eV of collision energy).

Pulse Amplitude–Modulated Measurements and Determination of Chlorophyll Content

The relative quantum efficiency of chlorophyll fluorescence was measured with 30-d-old tumors and inflorescence stalks using a MINI-PAM photosynthesis yield analyzer (Heinz Walz). Chlorophyll content was determined according to Arnon (1949).

Measurements of Oxygen Uptake and Protein Content

Polarographic measurements of oxygen uptake were performed with a Clark-type oxygen electrode (Hansatech Instruments). Tumor and inflorescence stalk tissue fragments of 2 to 3 mm were submerged in 10 mM $CaSO_4$, and their O_2 consumption was recorded for 8 min. Three samples were measured, containing tissue fragments from at least three plants. Protein content of tumor and inflorescence stalk tissue was determined using the BSA protein assay (Pierce).

Determination of Nitrate Reductase Activity

Nitrate reductase activity was determined from ~300 mg of frozen tissue of tumors without stalk or tumor-free stalks as described previously (Kaiser and Brendle-Behnisch 1995).

Supplemental Data

The following materials are available in the online version of this article.

Supplemental Figure 1. Distribution of All Differentially Expressed Genes within Functional Categories.

Supplemental Figure 2. Distribution of Differentially Expressed Genes of Three Functional Categories within Functional Subcategories.

Supplemental Figure 3. Verification of Differentially Expressed Genes by Quantitative RT-PCR after Affymetrix ATH1 Microarray Analysis.

Supplemental Figure 4. Verification of the Reproducibility of Affymetrix ATH1 Microarray Analysis.

Supplemental Figure 5. Comparison of Expression Values of All Affymetrix ATH1 Microarray Slides Applying Scatterplot Analysis.

Supplemental Table 1. Differentially Expressed Genes Upregulated in *Agrobacterium*-Induced Tumors of *Arabidopsis*.

Supplemental Table 2. Differentially Expressed Genes Downregulated in *Agrobacterium*-Induced Tumors of *Arabidopsis*.

Supplemental Table 3. Three Subtables of Differentially Expressed Genes of *Agrobacterium*-Induced *Arabidopsis* Tumors versus Tumor-Free Inflorescence Stalk Tissue.

Supplemental Table 4. Functional Categories of Differentially Expressed Genes Calculated from *Arabidopsis* Tumors Induced by *Agrobacterium* versus Reference Inflorescence Stalks.

Supplemental Table 5. Subcategories of Differentially Expressed Genes of the Functional Category of Primary Metabolism.

Supplemental Table 6. Subcategories of Differentially Expressed Genes of the Functional Category of Photosynthesis.

Supplemental Table 7. Subcategories of Differentially Expressed Genes of the Functional Category of Transport.

Supplemental Table 8. Comparison of Tumor- and Phytohormone-Dependent Gene Expression.

ACKNOWLEDGMENTS

We are grateful to Sean T. May (University of Nottingham, UK) for performing Affymetrix (ATH1) gene chip analyses. Special thanks go to

M. Lesch, E. Reissberg, E. Wirth, and J. Schwartz (Julius-von-Sachs-Institute, University of Wuerzburg) for excellent technical support on enzyme activity and metabolite measurements as well as to Biju Joseph (Department of Microbiology, University of Wuerzburg) for reading the manuscript. Finally, we thank M. Stitt (Max-Planck-Institute for Molecular Plant Physiology, Golm) for fruitful discussions. For generous financial support, we thank the Deutsche Forschungsgemeinshaft (SPP1063 project BO 1099/5 and SFB567 project B5), the Bundesministerium für Bildung und Forschung (IZKF B-36), and the European Union Biotechnology Program.

Received June 8, 2006; revised October 20, 2006; accepted November 10, 2006; published December 15, 2006.

REFERENCES

Aisenberg, A.C. (1961). The Glycolysis and Respiration of Tumors. (New York: Academic Press).

Aloni, R., Schwalm, K., Langhans, M., and Ullrich, C.I. (2003). Gradual shifts in sites of free-auxin production during leaf-primordium development and their role in vascular differentiation and leaf morphogenesis in *Arabidopsis*. Planta **216,** 841–853.

Amasino, R.M., Powell, A.L.T., and Gordon, M.P. (1984). Changes in T-DNA methylation and expression are associated with phenotypic variation and plant-regeneration in a crown gall tumor line. Mol. Gen. Genet. **197,** 437–446.

An, Y.Q., McDowell, J.M., Huang, S.R., McKinney, E.C., Chambliss, S., and Meagher, R.B. (1996). Strong, constitutive expression of the *Arabidopsis* ACT2/ACT8 actin subclass in vegetative tissues. Plant J. **10,** 107–121.

Arnon, D.I. (1949). Copper enzymes in isolated chloroplasts—Polyphenoloxidase in *Beta vulgaris*. Plant Physiol. **24,** 1–15.

Arruda, P., Kemper, E.L., Papes, F., and Leite, A. (2000). Regulation of lysine catabolism in higher plants. Trends Plant Sci. **5,** 324–330.

Benjamini, Y., and Hochberg, Y. (2000). On the adaptive control of the false discovery rate in multiple testing with independent statistics. Journal of Educational and Behavioral Statistics **25,** 60–83.

Carmeliet, P., and Jain, R.K. (2000). Angiogenesis in cancer and other diseases. Nature **407,** 249–257.

Chang, S., Lee, S., Lee, C., Kim, J.I., and Kim, Y. (2000). Expression of the human erythrocyte glucose transporter in transitional cell carcinoma of the bladder. Urology **55,** 448–452.

Chilton, M.D., Drummond, M.H., Merio, D.J., Sciaky, D., Montoya, A.L., Gordon, M.P., and Nester, E.W. (1977). Stable incorporation of plasmid DNA into higher plant cells: The molecular basis of crown gall tumorigenesis. Cell **11,** 263–271.

Cnops, G., et al. (2006). The TORNADO1 and TORNADO2 genes function in several patterning processes during early leaf development in *Arabidopsis thaliana*. Plant Cell **18,** 852–866.

Deeken, R., Ivashikina, N., Czirjak, T., Philippar, K., Becker, D., Ache, P., and Hedrich, R. (2003). Tumour development in *Arabidopsis thaliana* involves the Shaker-like K^+ channels AKT1 and AKT2/3. Plant J. **34,** 778–787.

Dessaux, Y., Petit, A., Tempe, J., Demarez, M., Legrain, C., and Wiame, J.M. (1986). Arginine catabolism in *Agrobacterium* strains—Role of the Ti-plasmid. J. Bacteriol. **166,** 44–50.

Ditt, R.F., Kerr, K.F., de Figueiredo, P., Delrow, J., Comai, L., and Nester, E.W. (2006). The *Arabidopsis thaliana* transcriptome in response to *Agrobacterium tumefaciens*. Mol. Plant Microbe Interact. **19,** 665–681.

Eastmond, P.J., and Graham, I.A. (2003). Trehalose metabolism: A regulatory role for trehalose-6-phosphate? Curr. Opin. Plant Biol. **6,** 231–235.

Eastmond, P.J., Li, Y., and Graham, I.A. (2003). Is trehalose-6-phosphate a regulator of sugar metabolism in plants? J. Exp. Bot. **54,** 533–537.

Fellenberg, K., Hauser, N.C., Brors, B., Neutzner, A., Hoheisel, J.D., and Vingron, M. (2001). Correspondence analysis applied to microarray data. Proc. Natl. Acad. Sci. USA **98,** 10781–10786.

Folkman, J. (1971). Tumor angiogenesis: Therapeutic implications. N. Engl. J. Med. **285,** 1182–1186.

Geisler, M., et al. (2005). Cellular efflux of auxin catalyzed by the *Arabidopsis* MDR/PGP transporter AtPGP1. Plant J. **44,** 179–194.

Geisler, M., and Murphy, A.S. (2006). The ABC of auxin transport: The role of p-glycoproteins in plant development. FEBS Lett. **580,** 1094–1102.

Gelvin, S.B., Karcher, S.J., and Dirita, V.J. (1983). Methylation of the T-DNA in *Agrobacterium tumefaciens* and in several crown gall tumors. Nucleic Acids Res. **11,** 159–174.

Gentleman, R., et al. (2004). Bioconductor: Open software development for computational biology and bioinformatics. Genome Biol. **5:R80** (http://genomebiology.com/2004–5/10/R80).

Gimbrone, M.A., Jr., Cotran, R.S., Leapman, S.B., and Folkman, J. (1974). Tumor growth and neovascularization: An experimental model using the rabbit cornea. J. Natl. Cancer Inst. **52,** 413–427.

Huber, W., Von Heydebreck, A., Sültmann, H., Poustka, A., and Vingron, M. (2002). Variance stabilization applied to microarray data calibration and to the quantification of differential expression. Bioinformatics **18,** S96–S104.

Ihaka, R., and Gentleman, R. (1996). R: A language for data analysis and graphics. J. Comput. Graph. Stat. **5,** 299–314.

Irizarry, R.A., Hobbs, B., Collin, F., Beazer-Barclay, Y.D., Antonellis, K.J., Scherf, U., and Speed, T.P. (2003). Exploration, normalization, and summaries of high density oligonucleotide array probe level data. Biostatistics **4,** 249–264.

Kachroo, A., Lapchyk, L., Fukushige, H., Hildebrand, D., Klessig, D., and Kachroo, P. (2003). Plastidial fatty acid signaling modulates salicylic acid- and jasmonic acid-mediated defense pathways in the Arabidopsis *ssi2* mutant. Plant Cell **15,** 2952–2965.

Kachroo, A., Venugopal, S.C., Lapchyk, L., Falcone, D., Hildebrand, D., and Kachroo, P. (2004). Oleic acid levels regulated by glycerolipid metabolism modulate defense gene expression in *Arabidopsis*. Proc. Natl. Acad. Sci. USA **101,** 5152–5157.

Kachroo, P., Shanklin, J., Shah, J., Whittle, E.J., and Klessig, D.F. (2001). A fatty acid desaturase modulates the activation of defense signaling pathways in plants. Proc. Natl. Acad. Sci. USA **98,** 9448–9453.

Kado, C.I. (1984). Phytohormone-mediated tumorigenesis by plant pathogenic bacteria. In Genes Involved in Microbe-Plant Interactions, D.P.S. Verma and T. Hohn, eds (Heidelberg, Germany: Springer Verlag), pp. 311–336.

Kaiser, W.M., and Brendle-Behnisch, E. (1995). Acid-base-modulation of nitrate reductase in leaf tissues. Planta **196,** 1–6.

Karchi, H., Shaul, O., and Galili, G. (1994). Lysine synthesis and catabolism are coordinately regulated during tobacco seed development. Proc. Natl. Acad. Sci. USA **91,** 2577–2581.

Kemp, J.D., Sutton, D.W., and Hack, E. (1979). Purification and characterization of the crown gall specific enzyme nopaline synthase. Biochemistry **18,** 3755–3760.

Kinnersley, A.M., and Turano, F.J. (2000). Gamma aminobutyric acid (GABA) and plant responses to stress. CRC Crit. Rev. Plant Sci. **19,** 479–509.

Kirsch, C., Takamiya-Wik, M., Reinold, S., Hahlbrock, K., and Somssich, I.E. (1997). Rapid, transient, and highly localized induction of plastidial omega-3 fatty acid desaturase mRNA at fungal infection sites in *Petroselinum crispum*. Proc. Natl. Acad. Sci. USA **94,** 2079–2084.

Kiyosue, T., Yoshiba, Y., Yamaguchi-Shinozaki, K., and Shinozaki, K. (1996). A nuclear gene encoding mitochondrial proline dehydrogenase, an enzyme involved in proline metabolism, is upregulated by proline but downregulated by dehydration in *Arabidopsis*. Plant Cell **8,** 1323–1335.

Klok, E.J., Wilson, I.W., Wilson, D., Chapman, S.C., Ewing, R.M., Somerville, S.C., Peacock, W.J., Dolferus, R., and Dennis, E.S. (2002). Expression profile analysis of the low-oxygen response in *Arabidopsis* root cultures. Plant Cell **14,** 2481–2494.

Kunst, L., and Samuels, A.L. (2003). Biosynthesis and secretion of plant cuticular wax. Prog. Lipid Res. **42,** 51–80.

Kursteiner, O., Dupuis, I., and Kuhlemeier, C. (2003). The Pyruvate decarboxylase1 gene of Arabidopsis is required during anoxia but not other environmental stresses. Plant Physiol. **132,** 968–978.

Maldonado, A.M., Doerner, P., Dixon, R.A., Lamb, C.J., and Cameron, R.K. (2002). A putative lipid transfer protein involved in systemic resistance signalling in *Arabidopsis*. Nature **419,** 399–403.

Malsy, S., Van Bel, A.J.E., Kluge, M., Hartung, W., and Ullrich, C.I. (1992). Induction of crown galls by *Agrobacterium tumefaciens* (strain C58) reverse assimilate translocation and accumulation in *Kalanchoë daigremontiana*. Plant Cell Environ. **15,** 519–529.

Mistrik, I., Pavlovkin, J., Wachter, R., Pradel, K.S., Schwalm, K., Hartung, W., Mathesius, U., Stohr, C., and Ullrich, C.I. (2000). Impact of *Agrobacterium tumefaciens*-induced stem tumors on NO_3-uptake in *Ricinus communis*. Plant Soil **226,** 87–98.

Mueller, M.J., Mene-Saffrane, L., Grun, C., Karg, K., and Farmer, E.E. (2006). Oxylipin analysis methods. Plant J. **45,** 472–489.

Ooms, G., Bakker, A., Molendijk, L., Wullems, G.J., Gordon, M.P., Nester, E.W., and Schilperoort, R.A. (1982). T-DNA organization in homogeneous and heterogeneous octopine-type crown gall tissues of *Nicotiana tabacum*. Cell **30,** 589–597.

Otto, B., and Kaldenhoff, R. (2000). Cell-specific expression of the mercury-insensitive plasma-membrane aquaporin NtAQP1 from *Nicotiana tabacum*. Planta **211,** 167–172.

Pedersen, P.L. (1978). Tumor mitochondria and the bioenergetics of cancer cells. Prog. Exp. Tumor Res. **22,** 190–274.

Pego, J.V., Kortstee, A.J., Huijser, G., and Smeekens, S.G.M. (2000). Photosynthesis, sugars and the regulation of gene expression. J. Exp. Bot. **51,** 407–416.

Peng, Z., Lu, Q., and Verma, D.P. (1996). Reciprocal regulation of delta 1-pyrroline-5-carboxylate synthetase and proline dehydrogenase genes controls proline levels during and after osmotic stress in plants. Mol. Gen. Genet. **253,** 334–341.

Pradel, K.S., Rezmer, C., Krausgrill, S., Rausch, T., and Ullrich, C.I. (1996). Evidence for symplastic phloem unloading with concomitant high activity of acid cell wall invertase in *Agrobacterium tumefaciens*-induced plant tumors. Bot. Acta **109,** 397–404.

Pradel, K.S., Ullrich, C.I., Santa Cruz, S., and Oparka, K.J. (1999). Symplastic continuity in *Agrobacterium tumefaciens* induced tumours. J. Exp. Bot. **50,** 183–192.

Rezmer, C., Schlichting, R., Wachter, R., and Ullrich, C.I. (1999). Identification and localization of transformed cells in *Agrobacterium tumefaciens*-induced plant tumors. Planta **209,** 399–405.

Risau, W. (1990). Angiogenic growth factors. Prog. Growth Factor Res. **2,** 71–79.

Rolland, F., Winderickx, J., and Thevelein, J.M. (2001). Glucose-sensing mechanisms in eukaryotic cells. Trends Biochem. Sci. **26,** 310–317.

Ryu, S.B. (2004). Phospholipid-derived signaling mediated by phospholipase A in plants. Trends Plant Sci. **9,** 229–235.

Sacristan, M.D., and Melchers, G. (1977). Regeneration of plants from habituated and *Agrobacterium*-transformed single-cell clones of tobacco. Mol. Gen. Genet. **152,** 111–117.

Scarpella, E., Marcos, D., Friml, J., and Berleth, T. (2006). Control of leaf vascular patterning by polar auxin transport. Genes Dev. **20,** 1015–1027.

Schreiber, U., Schliwa, U., and Bilger, W. (1986). Continuous recording of photochemical and nonphotochemical chlorophyll fluorescence quenching with a new type of modulation fluorometer. Photosynth. Res. **10,** 51–62.

Schurr, U., Schuberth, B., Aloni, R., Pradel, K.S., Schmundt, D., Jaehne, B., and Ullrich, C.I. (1996). Structural and functional evidence for xylem-mediated water transport and high transpiration in *Agrobacterium tumefaciens*-induced tumors of *Ricinus communis*. Bot. Acta **109,** 405–411.

Sheen, J., Zhou, L., and Jang, J.C. (1999). Sugars as signaling molecules. Curr. Opin. Plant Biol. **2,** 410–418.

Smeekens, S. (2000). Sugar-induced signal transduction in plants. Annu. Rev. Plant Physiol. Plant Mol. Biol. **51,** 49–81.

Smyth, G.K. (2004). Linear models and empirical Bayes methods for assessing differential expression in microarray experiments. Stat. Applic. Genet. Mol. Biol. **3,** Article 3 (http://www.bepress.com/sagmb/vol3/iss1/art3/).

Sousa, C., De Ferreira, A., and Sodek, L. (2002). The metabolic response of plants to oxygen deficiency. Braz. J. Plant Physiol. **14,** 83–94.

Suleiman, S., Hourmant, A., and Penot, M. (1990). Influence de l'acide abscissique sur le transport d'ions inorganiques chez la pomme de terre (*Solanum tuberosum* cv. Bintje). Etude comparée avec quelques autres phytohormones. Biol. Plant. (Praha) **32,** 128–137.

Szyroki, A., Ivashikina, N., Dietrich, P., Roelfsema, M.R.G., Ache, P., Reintanz, B., Deeken, R., Godde, M., Felle, H., Steinmeyer, R., Palme, K., and Hedrich, R. (2001). KAT1 is not essential for stomatal opening. Proc. Natl. Acad. Sci. USA **98,** 2917–2921.

Tadege, M., Dupuis, I., and Kuhlemeier, C. (1999). Ethanolic fermentation: New functions for an old pathway. Trends Plant Sci. **4,** 320–325.

Thimm, O., Blasing, O., Gibon, Y., Nagel, A., Meyer, S., Kruger, P., Selbig, J., Muller, L.A., Rhee, S.Y., and Stitt, M. (2004). MAPMAN: A user-driven tool to display genomics data sets onto diagrams of metabolic pathways and other biological processes. Plant J. **37,** 914–939.

Truernit, E., Schmid, J., Epple, P., Illig, J., and Sauer, N. (1996). The sink-specific and stress-regulated *Arabidopsis STP4* gene: Enhanced expression of a gene encoding a monosaccharide transporter by wounding, elicitors, and pathogen challenge. Plant Cell **8,** 2169–2182.

Ullrich, C.I., and Aloni, R. (2000). Vascularization is a general requirement for growth of plant and animal tumours. J. Exp. Bot. **51,** 1951–1960.

Usadel, B., et al. (2005). Extension of the visualization tool MapMan to allow statistical analysis of arrays, display of corresponding genes, and comparison with known responses. Plant Physiol. **138,** 1195–1204.

Van Larebeke, N., Engler, G., Holsters, M., Van den Elsacker, S., Zaenen, I., Schilperoort, R.A., and Schell, J. (1974). Large plasmid in *Agrobacterium tumefaciens* essential for crown gall-inducing ability. Nature **252,** 169–170.

Van Slogteren, G.M.S., Hoge, J.H.C., Hooykaas, P.J.J., and Schilperoort, R.A. (1983). Clonal analysis of heterogeneous crown gall tumor tissues induced by wild-type and shooter mutant strains of *Agrobacterium tumefaciens* expression of T-DNA genes. Plant Mol. Biol. **2,** 321–333.

Veselov, D., Langhans, M., Hartung, W., Aloni, R., Feussner, I., Gotz, C., Veselova, S., Schlomski, S., Dickler, C., Bachmann, K., and Ullrich, C.I. (2003). Development of *Agrobacterium tumefaciens*

C58-induced plant tumors and impact on host shoots are controlled by a cascade of jasmonic acid, auxin, cytokinin, ethylene and abscisic acid. Planta **216,** 512–522.

Wachsberger, P.R., Gressen, E.L., Bhala, A., Bobyock, S.B., Storck, C., Coss, R.A., Berd, D., and Leeper, D.B. (2002). Variability in glucose transporter-1 levels and hexokinase activity in human melanoma. Melanoma Res. **12,** 35–43.

Wachter, R., et al. (2003). Vascularization, high-volume solution flow, and localized roles for enzymes of sucrose metabolism during tumorigenesis by *Agrobacterium tumefaciens*. Plant Physiol. **133,** 1024–1037.

Wang, X.M. (2004). Lipid signaling. Curr. Opin. Plant Biol. **7,** 329–336.

Warburg, O. (1930). The Metabolism of Tumors. (London: Arnold Constable).

Weil, M., and Rausch, T. (1990). Cell wall invertase in tobacco crown gall cells: Enzyme properties and regulation by auxin.. Plant Physiol. **94,** 1575–1581.

West, C.E., Waterworth, W.M., Stephens, S.M., Smith, C.P., and Bray, C.M. (1998). Cloning and functional characterisation of a peptide transporter expressed in the scutellum of barley grain during the early stages of germination. Plant J. **15,** 221–229.